Coordination Chemistry Reviews 254 (2010) 2311–2341

Contents lists available at ScienceDirect

Coordination Chemistry Reviews

journal homepage: www.elsevier.com/locate/ccr

Review

STM studies on porphyrins

Joe Otsuki*

College of Science and Technology, Nihon University, 1-8-14 Kanda Surugadai, Chiyoda-ku, Tokyo 101-8308, Japan

Contents

ARTICLE INFO

Article history:
Received 31 October 2009
Accepted 29 December 2009
Available online 7 January 2010

Keywords:
Electrochemical scanning tunneling microscopy
Highly oriented pyrolytic graphite
Porphyrins
Scanning tunneling microscopy
Ultrahigh vacuum scanning tunneling microscopy

ABSTRACT

Porphyrins are promising components to be used in molecular electronics due to their rich electronic/photonic properties. Preparation of supramolecular architectures of porphyrins on solid surfaces would constitute a basis for further development toward molecular circuitry or other constructs for molecular electronics applications. Assemblies on surfaces can be probed with scanning tunneling microscopy (STM) at submolecular resolutions to reveal the arrangements and conformations of molecules on an individual molecule basis. The electronic characteristics within a single porphyrin molecule can also be probed by means of the same technique. This review summarizes the status quo of STM studies on porphyrins on surfaces with regard to their assemblies, structures, and electronic properties at the single molecule level.

1. Introduction

A number of molecules behave as active or passive electronic components [1–5], which opens the possibility for molecular electronics, in which individual molecules work as functional com-

* Tel.: +81 3 3259 0817; fax: +81 3 3259 0817.
E-mail address: otsuki@chem.cst.nihon-u.ac.jp.

0010-8545/$ – see front matter © 2010 Elsevier B.V. All rights reserved.
doi:10.1016/j.ccr.2009.12.038

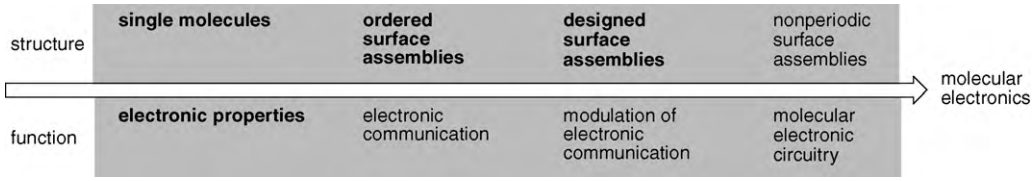

Fig. 1. Map toward molecular electronics. There are some achievements in the issues in bold-faced words, which are covered in this review, while those in plain letters are future challenges.

ponents. However, much research has to be done before realizing molecular electronics. Fig. 1 shows a simple map illustrating a way to reach the goal.

The first step is to know the structural and electronic properties of individual molecules. To investigate structures of assemblies formed from the component molecules may be the next step. Especially relevant are assemblies on surfaces, because connection between the molecular world and the macroscopic world will be achieved through conventional electronic circuitry constructed on solid substrates. Principles of higher order organization of molecules may be gleaned by analyzing the correlation between the structures of molecules and substrates and those of the assemblies thereof. Electronic communication among molecules within the assembly is of great importance as a basis for molecular electronic circuitry, although investigation in this direction is being hampered by technical difficulties. To go a step further, the art of molecular design must be mastered to create surface patterns by judicious choice of molecular shapes, polarities, distribution of hydrophilic/hydrophobic sites, as well as by incorporation of directional forces such as hydrogen bonding and coordination interactions. Many lessens can be learnt from supramolecular chemistry highly developed in three-dimensional realms [6,7]. In principle, electronic communication among molecules within the patterned assemblies is modulated from that in simpler close-packed assemblies. A much more challenging step that lies ahead is to construct nonperiodic assemblies. The top-down approach has been used to fabricate nonperiodic structures, whereas there seems to be no practical way from the bottom-up approach to nonperiodic assemblies at present. Nonperiodic assemblies of molecules may be required to realize molecular electronic circuits, however. Presently, we have excellent examples of studies on single molecules and their electronic properties, well-ordered surface assemblies, as well as designed surface assemblies, which are indicated by bold-faced words in Fig. 1 and are treated in this review.

Scanning tunneling microscopy (STM) provides a powerful means to study surface species at submolecular resolutions [8]. As the STM measures electric current through the tip and the substrate through the adsorbed molecule as a function of spatial position, the obtained data contain information on both the electronic structure and topographic structure. A number of excellent reviews are available, even in recent years only, on STM studies of molecular assemblies on surfaces from different perspectives [9–14]. Surface assemblies from porphyrins are of special interest, because porphyrins play important roles in processes ranging over electron transfer, energy transfer, light absorption, light emission, catalysis, and combinations of these both in nature and in artificial systems. In this review, STM studies on porphyrin molecules and molecular assemblies are summarized. The topics are organized mainly according to the substrates used. First, porphyrin assemblies on the surface of highly oriented pyrolytic graphite (HOPG) are described. Most of the STM studies using HOPG as a substrate are conducted under ambient conditions either at liquid/solid interfaces or air/solid interfaces. Second, porphyrin assemblies at interfaces of metals and electrolyte solutions studied with electrochemical STM (EC-STM) are described. The EC-STM enables the control of the substrate potential independent of the bias voltages. Third, porphyrin assemblies on metal surfaces with ultrahigh vacuum STM (UHV-STM) are described. The UHV conditions provide extremely clean surfaces, which would not be obtained at ambient conditions because of surface oxidation, etc. Wide temperature ranges can also be applicable for UHV-STM, which allows measurements at very low temperatures, making stable and high-resolution measurements possible. Therefore, the electronic structures of molecules and electronic processes occurring at the surfaces is mostly probed using UHV-STM.

2. Porphyrin assemblies on HOPG

2.1. HOPG

Using HOPG as a substrate for molecular assemblies for STM measurements has several advantages.

- HOPG has atomically flat surfaces.
- A clean surface is easily obtained by manual cleavage with adhesive tape.
- The surface is stable in air. This contrasts with most metal surfaces that often require high-vacuum conditions to keep the surface clean.
- HOPG is commercially available at an affordable price.

Surface assemblies are observed either at liquid/solid interface or air/solid interface. Since the initial observations of highly ordered arrays of liquid crystalline molecules on the HOPG surface [15–17], many studies have been devoted to various aspects of ordered arrays of molecules on the HOPG surface [18–22]. The most common strategy to obtain highly ordered assemblies of molecules on the HOPG surface is to use alkylated compounds taking advantage of their high affinities for the surface of HOPG. The high affinity originates from near commensurate packing of alkyl chains on the HOPG surface. Alkyl groups usually adopt the extended all-*trans* zigzag conformation. The primary driving force for the adsorption is van der Waals interactions between the alkyl groups and the HOPG surface. The secondary force involved in the packing is van der Waals interaction between alkyl groups [23]. It would be wise to pay attention to Moiré patterns and graphitic artifacts that could be mistaken for molecular assemblies before making any conclusions about exotic structures of molecular assemblies [24–28].

2.2. Assemblies of simple porphyrin derivatives on HOPG

STM studies on porphyrins adsorbed on HOPG were initially performed to reveal how these molecules adsorb on the surface as a model of electrocatalytic surfaces. Iron(III) protoporphyrin IX, zinc(II) protoporphyrin IX, and free-base protoporphyrin IX all lie flat and form two-dimensional densely packed lattices at the electrolyte solution/HOPG interface [29].

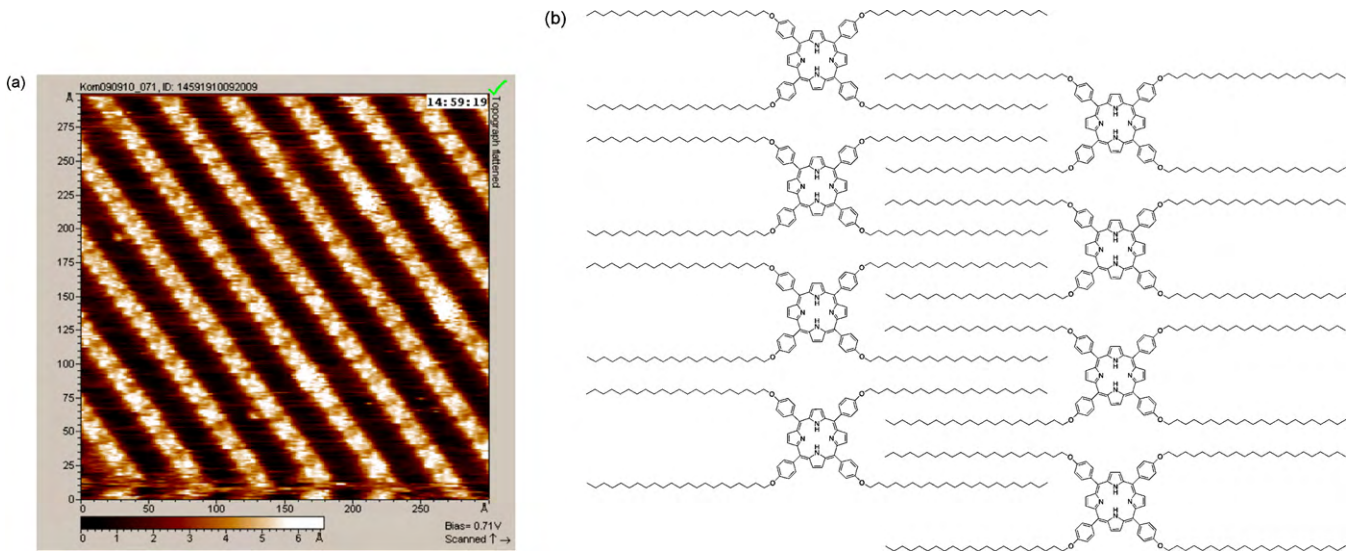

Fig. 2. Surface array of H_2-T(C_{22}OP)P at the 1-phenyloctane/HOPG interface. (a) STM image. (b) Molecular models.

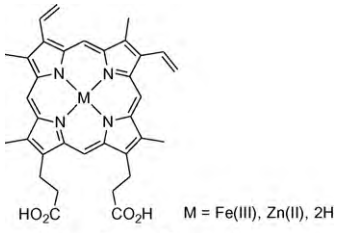

protoporphyrin IX

The close-packed assemblies are formed from intact protoporphyrin IX as described just above. Not all molecules form a packed array suitable for STM observation, however. The physical adsorption of small organic molecules to the surface of HOPG at ambient temperatures is not strong enough for an isolated molecule to be immobilized to allow STM observation. Molecules need to form a packed array. A general strategy to immobilize a molecule is to attach alkyl chains to the molecule of interest. Thus, surface assemblies of M-T(C_nOP)P molecules were realized at the 1-phenyloctane/HOPG interface and observed with STM under ambient conditions [30–32].

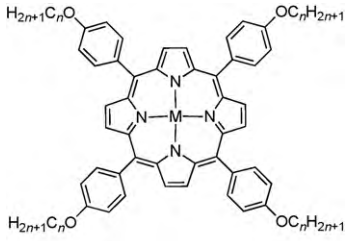

M-T(C_nOP)P

The tetrakis(alkoxy)phenyl porphyrins form a lamellar arrangement with alkyl chains from the porphyrin rows interdigitate, giving rise to a close-packed array. The image shown in Fig. 2 is the array of H_2-T(C_{22}OP)P at the 1-phenyloctane/HOPG interface. Each of the four-lobed structure corresponds to a molecule of porphyrin forming a lamellar arrangement. The bright lobes appear at the positions of the phenyl groups. In the area of dark troughs, alkyl chains extending nearly perpendicular to the molecular rows cover the surface. The interlamellar separation can be adjusted with the number of carbons in the alkyl chains.

The fabrication of desired surface two-dimensional patterns might be of importance to be used in a specific purpose, such as shape selective catalysis and a directional guidance of electrons along a specified route, to name a few. One way to obtain patterns other than close-packed structures may be to use directional forces such as hydrogen bonds and coordination bonds, as described below. Another way may be to introduce a perturbation on part of the alkyl chain. The surface assemblies made from porphyrins bearing alkyl chains each of which contains a diacetylene unit, M-T(C_nDAP)P, were examined in this context [33]. The diacetylene moiety imparts kinks in the middle of the alkyl chains. The diacetylene-containing porphyrin derivative with the longest alkyl chain (n = 15) forms a lamellar pattern on the surface of HOPG, with the porphyrin planes adopting a face-on orientation, as shown in Fig. 3a. The kinks in the alkyl chains prevent the formation of a close-packed structure, resulting in a less dense surface pattern with void spaces in the array. For the diacetylene-containing porphyrin derivatives with shorter alkyl chains (n = 9 and 4), the molecules form columns via ππ stacking of porphyrin macrocycles (Fig. 3b). The columns, which run parallel to the HOPG surface, align side-by-side to fill the surface. The porphyrin planes are in an edge-on orientation with respect to the substrate surface. Qualitatively, the final structure is determined by the balance between attractive interactions between porphyrin macrocycles via ππ stacking and another attractive interaction between alkyl chains and the surface of HOPG. Therefore, the face-on adsorption motif is preferred for porphyrins with longer alkyl chains, while column formation dominates for porphyrins with shorter alkyl chains.

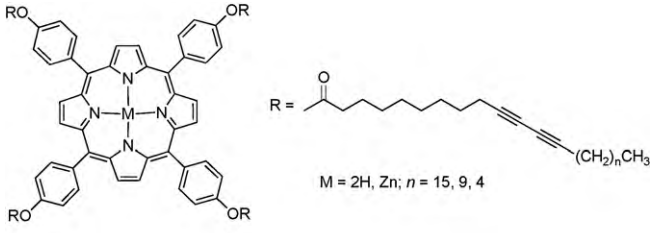

M-T(C_nDAP)P

The *meso*-phenyl rings make an angle with respect to the porphyrin plane in *meso*-tetraphenylporphyrin (TPP) derivatives [34]. This would prevent strong interactions between the porphyrin plane with the substrate. On the other hand, *meso*-tetraalkylporphyrin, M-TC$_n$P, has no such steric constraint and hence strong interactions between the porphyrin macrocycle and the substrate are anticipated. The free-base [35,36] and

copper–porphyrin [35] spontaneously self-assemble into extended arrays at the interface between HOPG and 1-phenyloctane or tetradecane. The packing of M-TC_{12}P molecules revealed by STM indicates that only two alkyl chains in the molecule are physisorbed on the surface of HOPG. The remaining alkyl chains are probably pointing away from the surface into the solution.

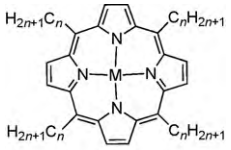

M-TC_nP

H_2-TC_{12}P molecules form a well-ordered monolayer assemblies also at the tetradecane/Au(1 1 1) interface [36]. Only one alkyl chain in each molecule is adsorbed in this case, maximizing the surface density of the molecules. The high density assembly suggests that the porphyrin macrocycle–surface interaction is more favorable than the alkyl chain–surface interaction for the gain in the free-energy of adsorption. Four-lobed structures are observed for H_2-TC_{12}P molecules in the STM image. It was suggested that the four-lobed image represents distortion of the porphyrin core of H_2-TC_{12}P out of planarity. The X-ray photoemission spectrum of the N 1s core level on the monolayer showed a peak that can be assigned to iminic nitrogen atoms (–C=N–) coordinated onto Au(1 1 1), in addition to those corresponding to pyrrolic nitrogen atoms (–NH–) and free iminic nitrogen atoms.

Scanning tunneling spectroscopy (STS) for the Cu-TC_{11}P at the Au(1 1 1)/tetradecane interface shows prominent peaks in differential current (dI/dV) at −0.175 and +0.300 V, which are within a range much narrower than the HOMO–LUMO gap of the Cu–porphyrin [35]. These peaks imply the presence of new binding states as a consequence of a strong porphyrin–substrate interaction.

Ni-OEP also forms ordered arrays on the surface of HOPG (from volatile organic solutions) and on Au(1 1 1) (vapor deposited) [37]. The molecules in the array on HOPG were manipulated with a STM tip to make an exposed HOPG surface in certain patterns [38]. The effects of chiral substituents on the structures of the assemblies were examined in detail with H_2-T(*R*-amideP)P [34,39]. Strapped porphyrin, M-T(C_{24}OP)P-strap, forms ordered arrays on the surface of HOPG, pointing to a possibility of making functional arrays via chemical modification on the strapped moiety [40].

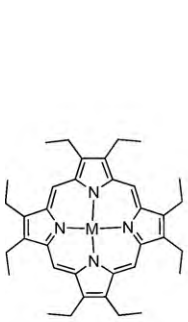

M-OEP

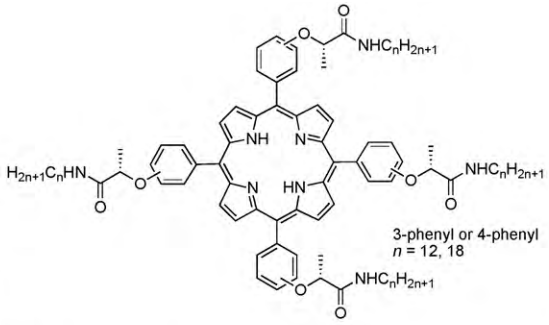

H_2-T(*R*-amideP)P

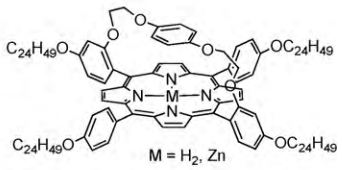

M-T(C_{24}OP)P-strap

2.3. Porphyrin assemblies governed by directional intermolecular interactions on HOPG

It is possible to design surface patterns other than close-packed structures by incorporating sites for directional interaction, such as hydrogen bonding and coordination interactions, into the molecular structure. A tris(alkoxyphenyl)porphyrin derivative with one hydroxyphenyl group left intact, Zn-(HOP)(C_{12}OP)$_3$P, assembles into patterns different from that formed from M-T(C_nOP)P [41]. Two different arrangements form. One is an arrangement in which the porphyrin adsorb face-on to the surface, forming dimeric units most likely through the formation of a hydrogen bond involving the hydroxyl group. A similar dimeric formation was also found in the monolayer of bacteriochlorophyllides c, which has a free hydroxyl group on the periphery of the macrocycle, deposited from a methanol solution on HOPG [42]. The other is a columnar assembly adsorbed on the surface in an edge-on orientation. The fact that these two patterns coexist means that the free-energy of formation for these completely different patterns happen to be close each other.

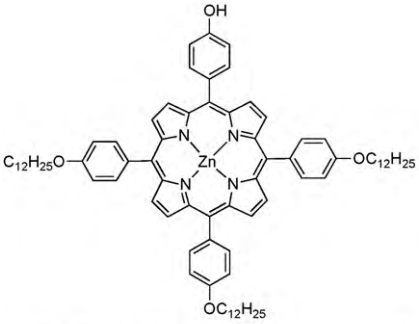

Zn-(HOP)(C_{12}OP)$_3$P

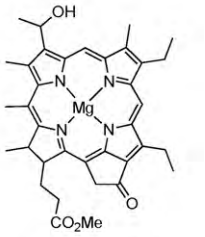

bacteriochlorophyllides c

Apart from their distinguished electronic and photonic properties, porphyrins are suitable as a model in examining the relationship between the molecular structures and the supramolecular structures, since substituents for intermolecular interactions can be synthetically introduced to the corners of square-shaped porphyrin scaffold in different numbers and positions in a systematic way. Effects of hydrogen bonding on the structures of surface assemblies were investigated with a series of TPP derivatives with a certain number of carboxyl groups on the phenyl moieties. The bulk crystal of Zn-T(HO_2CP)P consists of two-dimensional sheets stacked together, in which porphyrin molecules are connected through the hydrogen-bonded carboxylic acid cyclic dimer [43]. On the surface of HOPG, however, a different type of hydrogen bonding network forms from H_2-T(HO_2CP)P, which is joined by carboxylic acid tetramers (Fig. 4) [44]. The surface density is higher in this motif than in the sheet in the bulk crystals. The increased surface density is favorable with respect to molecule–surface interactions. Yet, the density is still lower than the close-packed structure to maintain the hydrogen bonds among the carboxyl groups even though they are not optimum ones. Thus, the molecule–substrate interactions perturbs the hydrogen bonding, giving rise to a new motif of two-dimensional array on the surface.

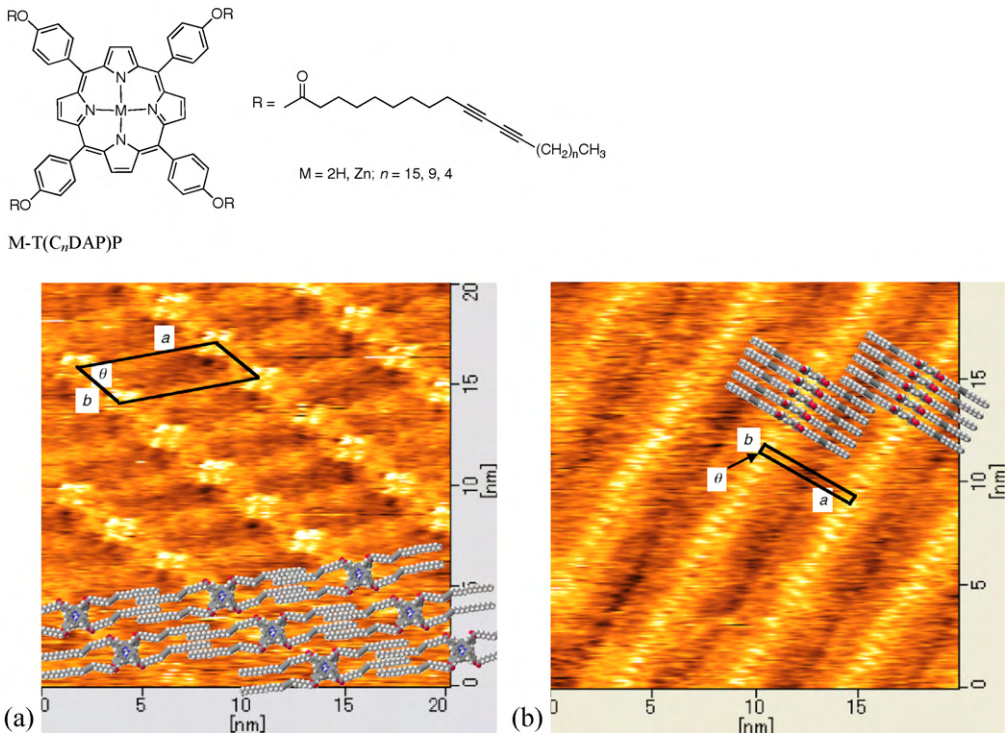

Fig. 3. Surface patterns formed from porphyrin derivatives bearing alkyl chains, each of which has a diacetylene moiety in the middle. (a) H_2-T(C_{15}DAP)P. Face-on arrangement. (b) H_2-T(C_9DAP)P. Columnar arrays, in which the porphyrins take an edge-on orientation. Reproduced with permission from Ref. [33].

TPP derivatives bearing both alkyl chains and carboxyl moieties at the 4-position of the phenyl groups in every possible combination were examined with regard to their self-assembled structures. Two of them, i.e., *cis*-H_2-(HO_2CP)$_2$(C_{18}OP)$_2$P and H_2-(HO_2CP)(C_{18}OP)$_3$P, afforded ordered arrays on HOPG [45]. In *cis*-H_2-(HO_2CP)$_2$(C_{18}OP)$_2$P, the carboxyl moieties are introduced on the two adjacent corners of the molecule. *cis*-H_2-(HO_2CP)$_2$(C_{18}OP)$_2$P molecules assemble into a motif of M-T(HO_2CP)P and M-T(C_nOP)P combined. It forms a lamellar structure, in which each row consists of a pair of porphyrins associated in a head-to-head configuration, as shown in Fig. 5a. Alkyl moieties are arranged in the same motif of interdigitation as in the array of T(C_nOP)P. Carboxyl moieties are arranged in the same motif of the cyclic hydrogen-bonded tetramer found for T(HO_2CP)P.

The array of H_2-(HO_2CP)(C_{18}OP)$_3$P is shown in Fig. 5b. The rows constituting the lamellar arrangement exhibits kinks. The kink may be attributed to the complementary hydrogen bond between the carboxyl groups from the adjacent molecules across the kink. This view is supported by the center-to-center distance of 2.5 nm between the pair of H_2-(HO_2CP)(C_{18}OP)$_3$P molecules across the kink, which agrees with the corresponding distance across the hydrogen-bonded carboxyl porphyrins in the bulk crystal structure [43]. The formation of the kinks reduces the surface density of molecules. This, in turn, results in the reduction in

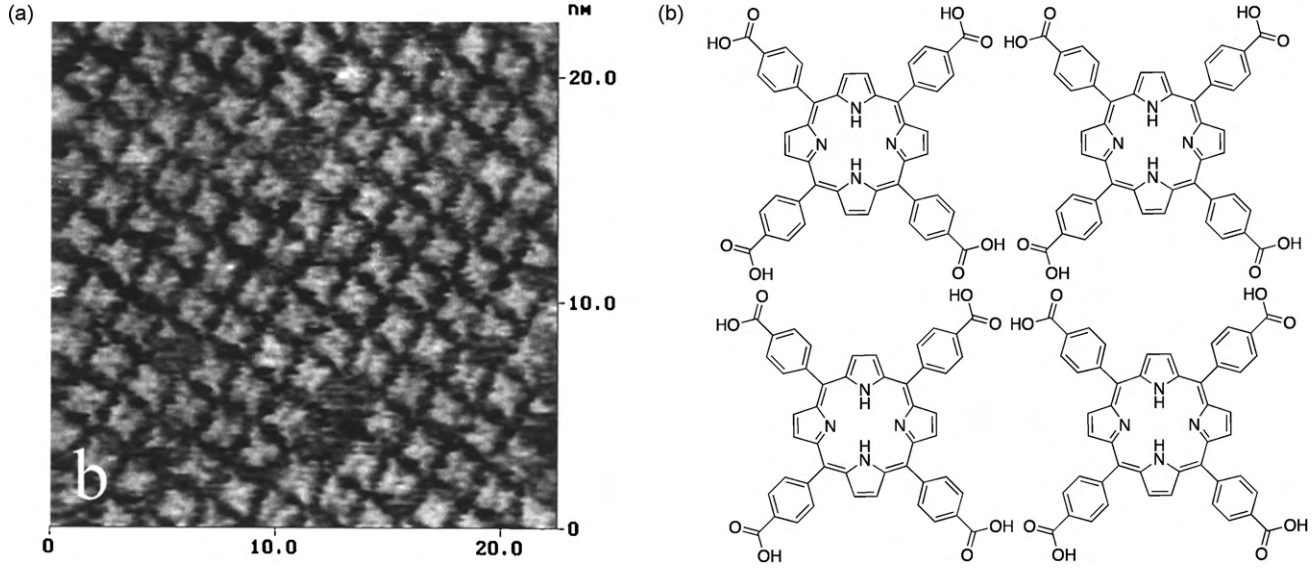

Fig. 4. Observed motif of hydrogen bonding network of Zn-T(HO_2CP)P on HOPG. (a) STM image. (b) Molecular arrangement. The packing is denser than in the two-dimensional sheet in the bulk crystal. Reproduced with permission from Ref. [44].

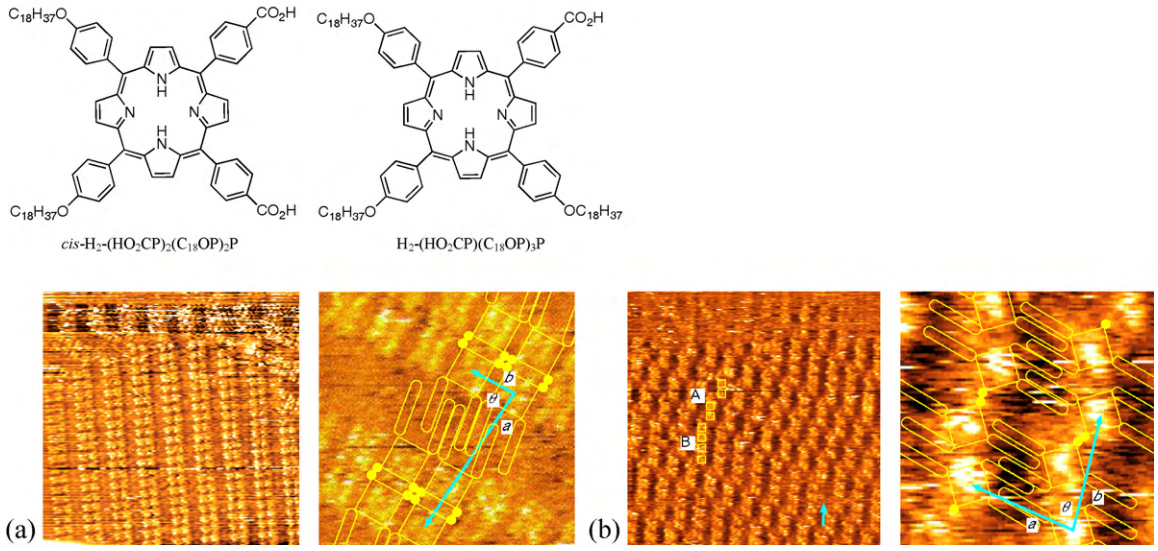

Fig. 5. STM images for *cis*-H_2-$(HO_2CP)_2(C_{18}OP)_2P$ (a) and H_2-$(HO_2CP)(C_{18}OP)_3P$ (b). Left images: 50 nm × 50 nm; right images: 10 nm × 10 nm. Reproduced with permission from Ref. [45].

molecule–substrate and molecule–molecule interactions. The loss must be outweighed by the gain obtained by the hydrogen bond formation. In some places kinks appear every other molecule (pattern A in Fig. 5b) but in other places more than two molecules are aligned linearly (pattern B). In the region of pattern B, packing forces apparently dominates over hydrogen bonding interactions. Thus, in the case of this particular molecule, it is inferred that packing forces and hydrogen bonding forces are in a subtle balance.

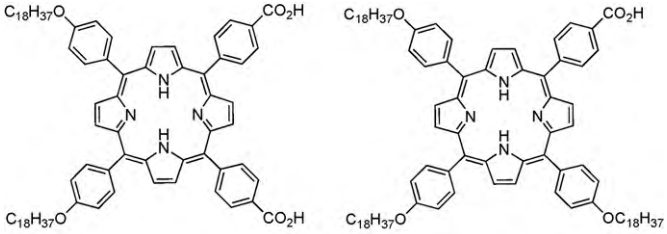

cis-H_2-$(HO_2CP)_2(C_{18}OP)_2P$ H_2-$(HO_2CP)(C_{18}OP)_3P$

There seem to be few examples of well-ordered surface assemblies whose structure is controlled with coordination interactions, which have been characterized by means of STM with a molecular resolution.

Planar and square nonameric assemblies of porphyrins have been realized in solution using the pyridyl–palladium coordination interaction (Fig. 6) [46–48]. The supramolecular structure is programmed into the structure of component molecules. Note that three different porphyrins spontaneously come together to be placed in specific positions, i.e., the center, the side, and the corner, of the resulting assembly, depending on the arrangements of the pyridyl groups. This nonamer was deposited onto various substrate surfaces, including glass, mica, and Au(1 1 1). The morphology of the resulting layer of the supramolecular species was characterized mainly with AFM. An isolated nonamer deposited on Au(1 1 1) was observed with STM, revealing its square shape.

Phenanthroline-strapped porphyrins bearing imidazole arms and alkyl chains, Zn-P-Im-strap, form dimers upon zinc(II) complexation in solution via mutual imidazole–zinc coordination [49]. On HOPG, the dimers transform into wire-like coordination polymers to maximize interactions between the alkyl chains and the HOPG surface as shown in Fig. 7. The morphology of the resulting assembly was characterized with AFM.

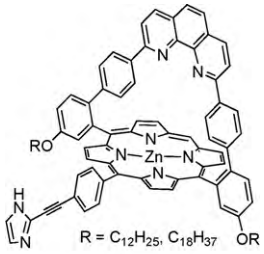

Zn-P-Im-strap

2.4. Assemblies of elaborate porphyrin derivatives on HOPG

Whereas two-dimensional assemblies of double- and triple-decker phthalocyanine derivatives have been extensively investigated, relatively a small number of studies on porphyrin counterparts have been reported. The surface assemblies were investigated for three double-decker complexes commonly having a $T(C_{22}OP)P$ ring: (Pc)Ce($T(C_{22}OP)P$), ($T(C_{22}OP)P$)Ce($T(C_{22}OP)P$), and (B(PEP)P)Ce($T(C_{22}OP)P$) [50]. All of these molecules respectively assemble into the lamellar arrangement at the 1-phenyloctane/HOPG interface with lattice parameters identical to that of $T(C_{22}OP)P$. This indicates that these double-decker complexes form the adlayers with the $T(C_{22}OP)P$ face adsorbed. The STM images for individual molecules reflect the shape of the upper ring. Thus, molecules of (Pc)Ce($T(C_{22}OP)P$), ($T(C_{22}OP)P$)Ce($T(C_{22}OP)P$), and (B(PEP)P)Ce($T(C_{22}OP)P$) appear as circular, square, and elliptic (Fig. 8a). As the lattice parameters are identical, H_2-$T(C_{22}OP)P$ and (B(PEP)P)Ce($T(C_{22}OP)P$) form mixed assemblies. Molecules of (B(PEP)P)Ce($T(C_{22}OP)P$) appeared elliptic when placed within their own row, while they appeared isotropic when flanked by H_2-$T(C_{22}OP)P$ molecules as shown in Fig. 8b. Within a row of (B(PEP)P)Ce($T(C_{22}OP)P$) molecules, the upper ring, B(PEP)P, must orient perpendicular to the row because there is no room for the upper ring to take parallel orientation, which would overlap the upper rings of the adjacent double-decker molecules. The elliptic features perpendicular to the molecular rows in the STM images are consistent with this view. However, for a (B(PEP)P)Ce($T(C_{22}OP)P$) molecule flanked by H_2-$T(C_{22}OP)P$ molecules, the upper ring can adopt the parallel orientation, in which the phenylethynyl groups lie above the neighboring H_2-$T(C_{22}OP)P$ molecules. Thus, the

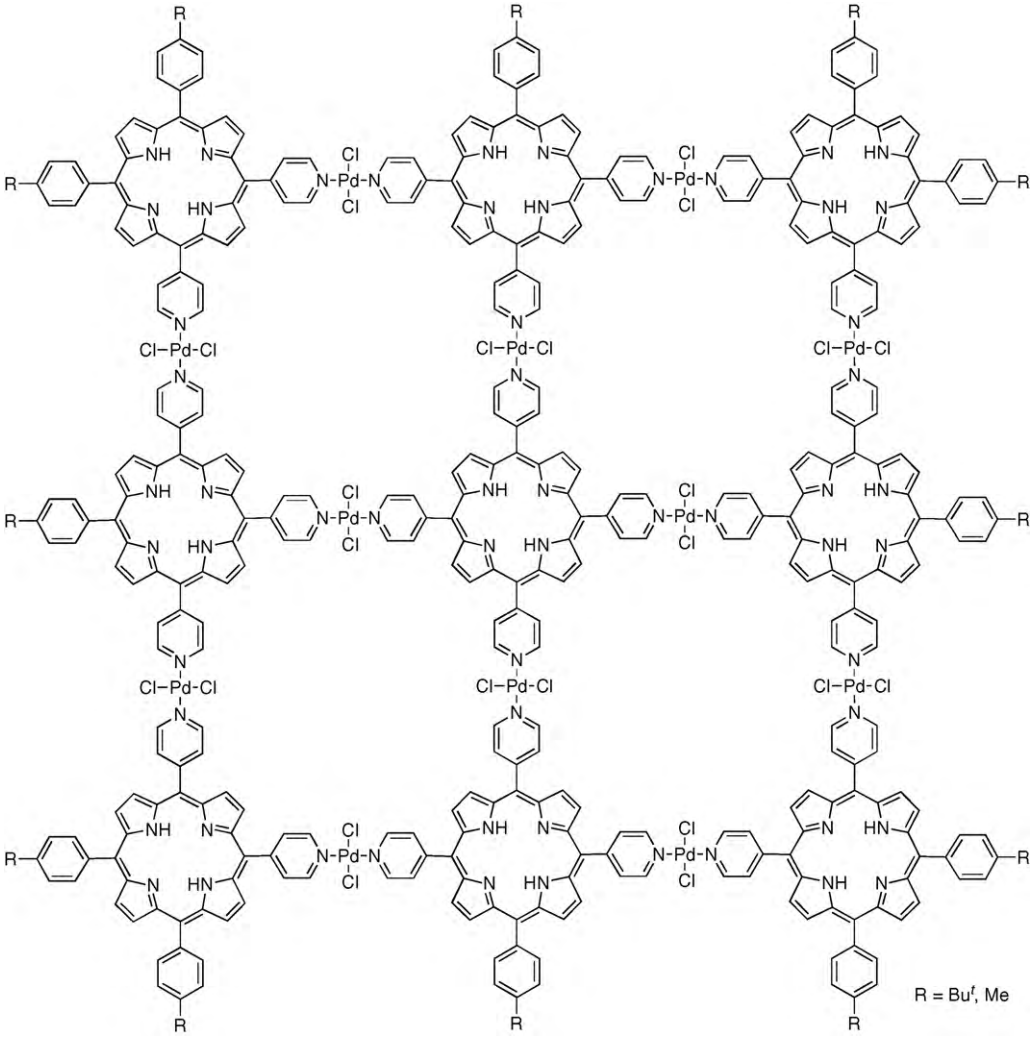

Fig. 6. Self-assembled nonameric porphyrin square [46–48].

observed isotropic shape in the STM images suggests that the upper ring is rotating faster than the STM time scale (it takes several seconds to complete the imaging for one molecule). Temperature varied ^{1}H NMR spectra for (B(PEP)P)Ce(T(C_{22}OP)P) showed that the inter-ring orientation change, i.e., a 90°-flip, occurs with a rate of ca. 3 s^{-1} in a solution phase at room temperature.

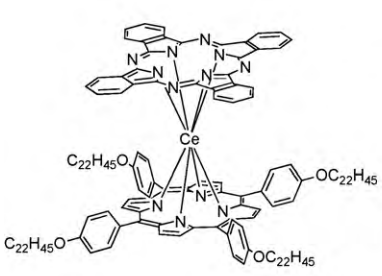

(Pc)Ce(T(C_{22}OP)P)

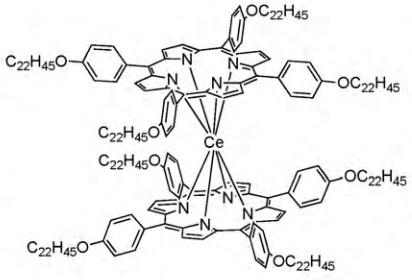

(T(C_{22}OP)P)Ce(T(C_{22}OP)P)

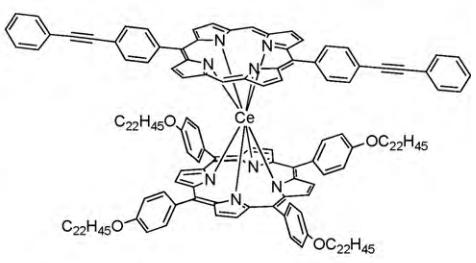

(B(PEP)P)Ce(T(C_{22}OP)P)

The structures formed from the three double-decker complexes having a naphthalocyanine ring as a common component were examined at the 1-phenyloctane/HOPG interface [51]. All these molecules form well-ordered arrays on HOPG with the naphthalocyanine ligands adsorbed onto the graphite surface. Hence the lattice parameters for these molecules are identical, which makes it possible to prepare ordered arrays from mixtures of these molecules. However, in the mixed array of (OEP)Lu(Nc) and (T(BP)P)Lu(Nc), these two molecules clearly segregated into bands forming striped patters along the [100] direction of the basal plane of graphite. Therefore, it is concluded that the upper rings have a subtle influence on the assembly structure even though the lattice constants are determined by the lower, adsorbed rings.

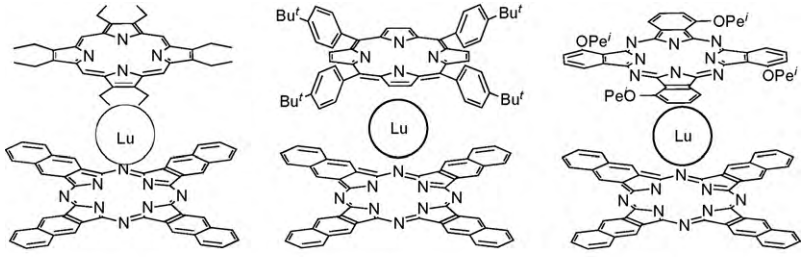

(OEP)Lu(Nc) (T(BP)P)Lu(Nc) (POPc)Lu(Nc)

Porphyrin hexamer, M-P_6, assembles into either face-on or edge-on adlayers at the 1-phenyloctane/HOPG interface [52]. Upon dropping a solution of H_2-P_6 on the surface of HOPG, kinetically favored face-on oriented structures form. These structures are, over a few hours, replaced by thermodynamically more favorable edge-on oriented columnar assemblies. For Zn-P_6, only the edge-on columnar assemblies are observed. The columnar assembly is favored because of ππ stacking interactions between the porphyrin macrocycles in the hexamer. It is well known that amines and pyridine derivatives axially coordinate to a zinc–porphyrin. The columnar structure of the assembly of Zn-P_6 is retained upon addition of diaza[2.2.2]bicyclooctane (DABCO). This is because the axial ligands are nicely accommodated between two zinc–porphyrin macrocycles of neighboring molecules, as shown in Fig. 9a. The ππ stacking interactions between the two molecules mutually face-to-face oriented remain even with DABCO in between. However, addition of 4,4′-bipyridine, which is too long to be accommodated between the ππ-stacked molecules, disrupts the ππ stacking interactions. As a result, a face-on oriented arrangement, which is not observed for Zn-P_6 alone without 4,4′-bipyridine, is observed as shown in Fig. 9b. Thus, the structure of molecular assembly changes dramatically by the presence of an additional chemical species.

An even larger porphyrin dodecamer, M-P_{12}, was synthesized and its surface assembly was investigated [53,54]. Spectroscopic and computational studies indicate that M-P_{12}, has a yo-yo-shaped structure. Whereas H_2-P_{12}, forms a columnar assembly with an edge-on orientation on the surface of HOPG, Zn-P_{12} does not form any stable assembly. Upon addition of DABCO, however, huge well-ordered domains of Zn-P_{12} molecules were observed, implying that DABCO stabilizes the surface assembly by working as a glue to bridge the neighboring dodecameric molecules. Zn-P_{12} forms an ordered array even in the presence of 4,4′-bipyridine as shown in Fig. 9c, unlike the case of Zn-P_6. The 4,4′-bipyridine molecules bridge the Zn-P_{12} molecules via zinc–pyridine coordination, defining the intermolecular distance in the surface array.

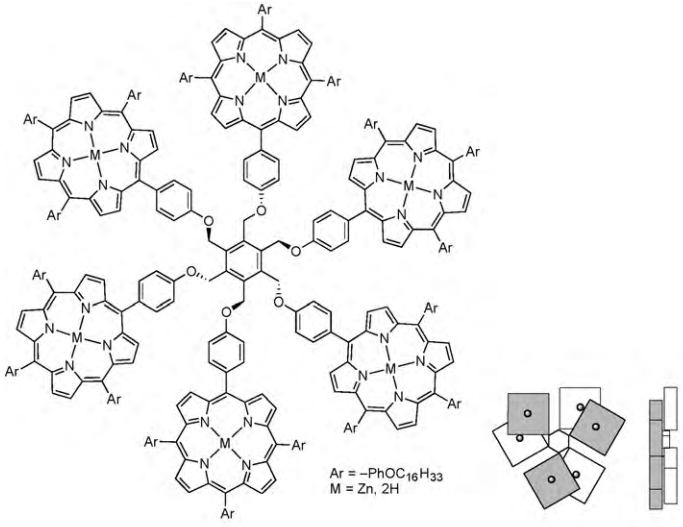

M-P_6

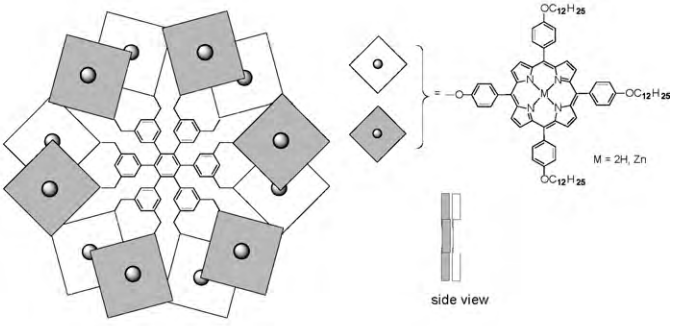

M-P_{12}

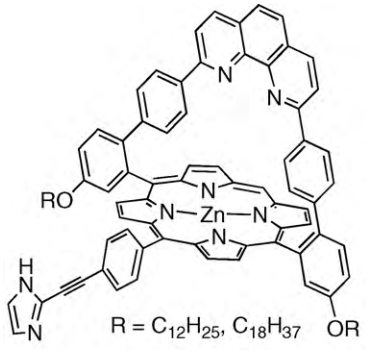

Zn-P-Im-strap

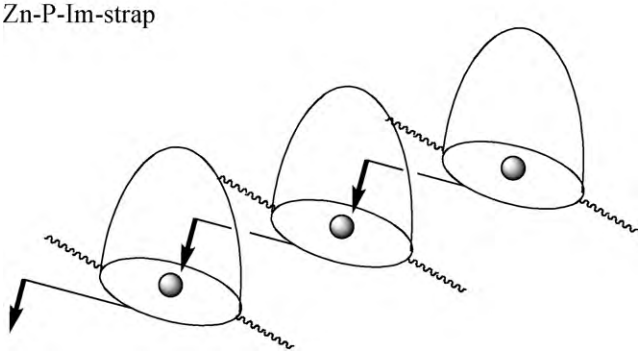

Fig. 7. Zn-P-Im-strap and its array via coordination interactions [49].

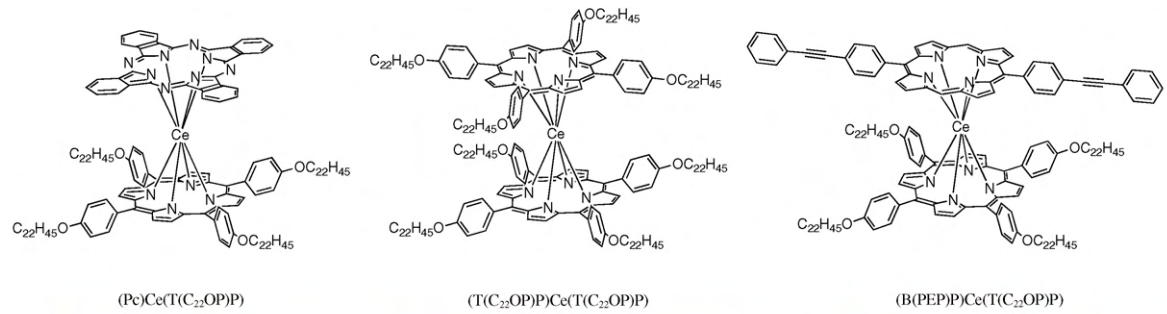

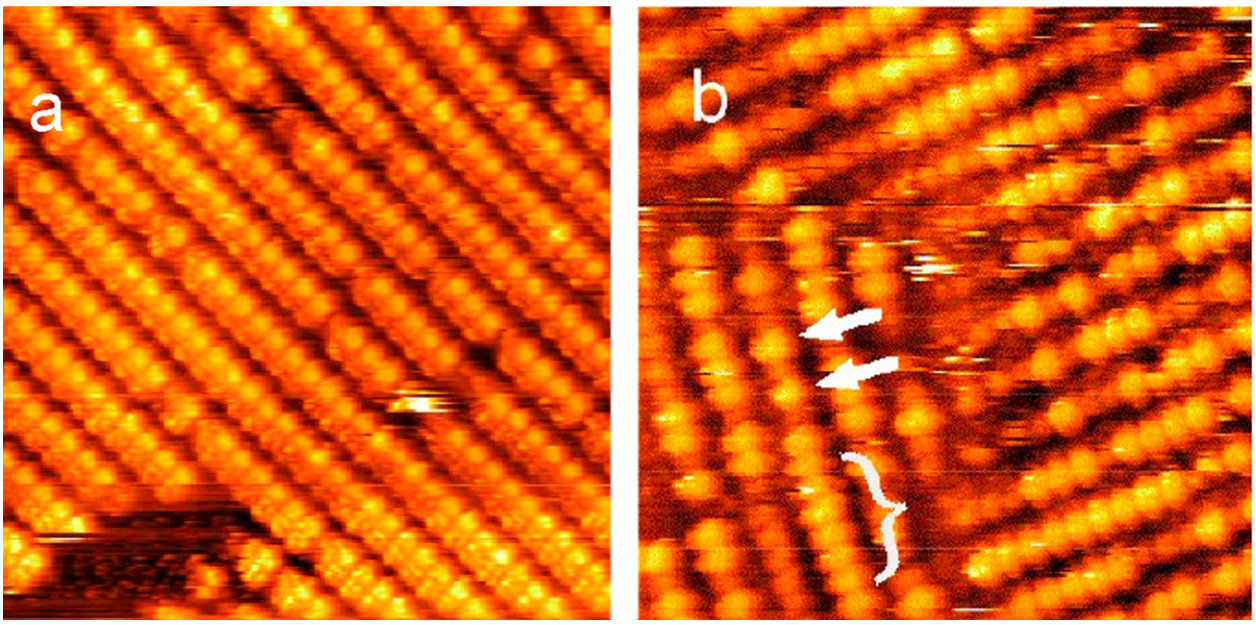

Fig. 8. STM images for double-decker complexes at the 1-phenyloctane/HOPG interface. 50 nm × 50 nm. (a) (B(PEP)P)Ce(T(C_{22}OP)P). (b) A mixed assembly of (B(PEP)P)Ce(T(C_{22}OP)P) and H_2-T(C_{22}OP)P. Note that spots are elliptic in rows consisting of the double-decker complexes (bracket), those for isolated double-decker complexes flanked by the free-base porphyrin molecules are more or less isotropic (arrows). Reproduced with permission from Ref. [50].

A covalent cyclic porphyrin box accommodating a tetrapyridyl porphyrin molecule via axial coordination, Zn-P_4·H_2-TPyP, assembles into highly ordered arrays on HOPG [55]. In this supramolecule, the accommodated H_2-TPyP worked as a template in the synthesis of the tetrameric box-like structure of Zn-P_4. The STM image indicates that the zinc porphyrins on the periphery of the box are oriented edge-on with respect to the surface, leaving the free-base porphyrin inside the box parallel to the surface. This topology maximized the number of stabilizing ππ interactions between neighboring zinc porphyrins in the two-dimensional array.

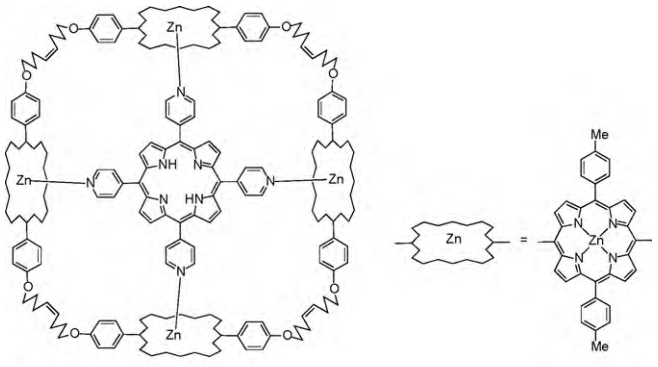

Zn-P_4·H_2-TPyP

2.5. Axial ligands on two-dimensional porphyrin assemblies on HOPG

Metal porphyrins can accommodate additional ligands axially coordinating to the central metal ions [56]. We have already seen several examples of axial coordination in supramolecular assemblies in previous sections. The ability to form ordered arrays on surfaces combined with the ability to accommodate an axial ligand makes porphyrins potential candidates for “a pedestal” on which functional moieties form ordered arrays. Functional molecules designed to have pyridine-like moieties for their immobilization on the metal porphyrins may be used. The surface arrangement can be designed by using suitably modified porphyrins for surface patterning. Thus, the properties of the functional moiety and the surface arrangement are independently designed in this modular approach.

Unlike the axial coordination of a pyridine derivative to a Zn–porphyrin, the coordination to Rh–porphyrin is much stronger. The bond between the pyridine and the rhodium ion is so strong that the coordinated species can be purified through a silica gel column. Thus, Rh–porphyrins are more suited to construct more stable surface assemblies. However, the preference of the rhodium ion toward six coordination prevents the formation of a desired five-coordinated species. The sixth ligand may hinder stable adsorption to the surface. In fact, RhCl-T(C_{18}O)P)P·Py does not form a stable monolayer on HOPG, because the chlorine atom protrudes out to prevent the phenyl groups from adsorbing on the surface in

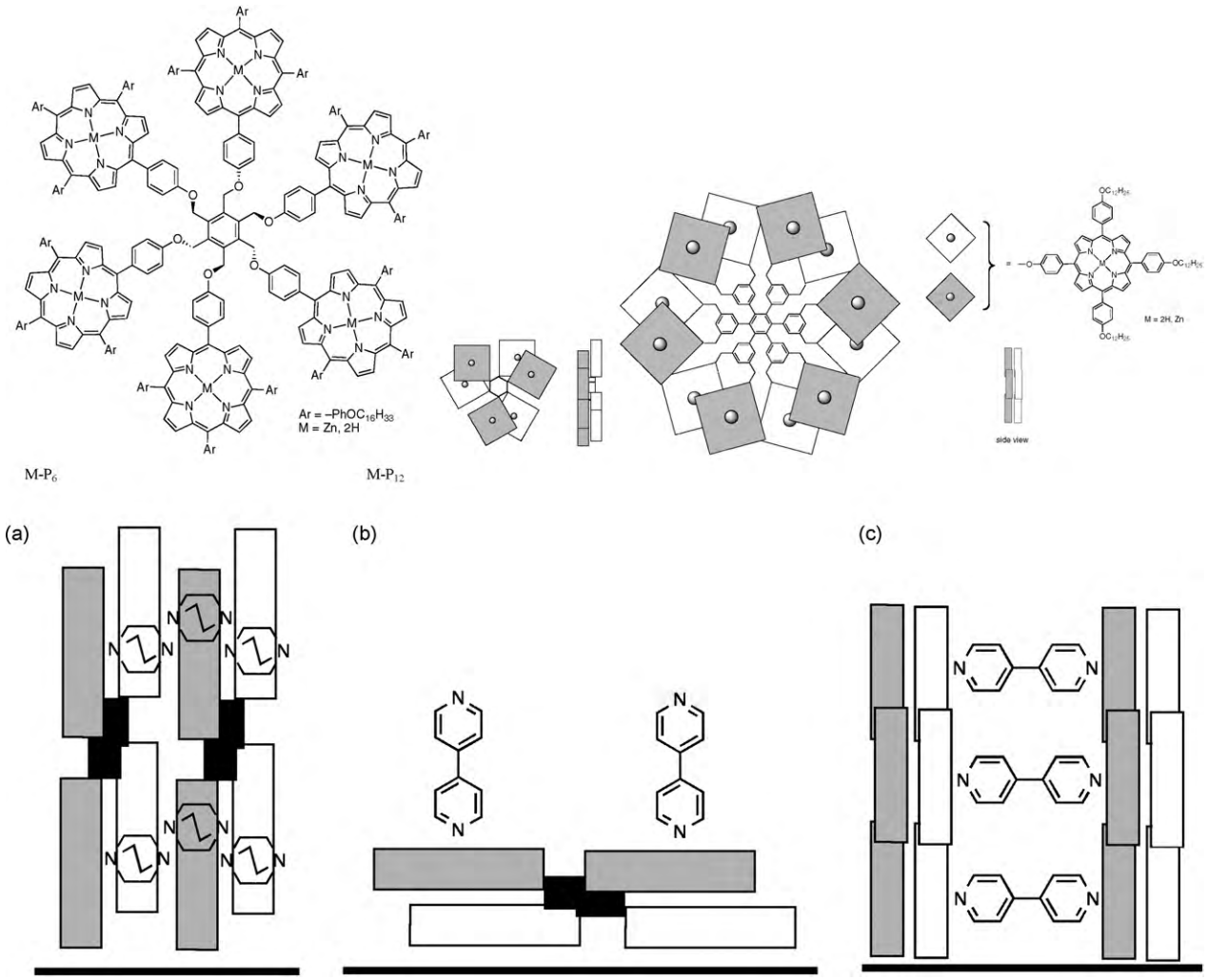

Fig. 9. Surface assemblies of the zinc–porphyrin hexamer [52] and dodecamer [53,54]. (a) Edge-on columnar assembly of Zn-P_6 incorporating DABCO. (b) 4,4′-Bipyridine disrupts the ππ stacking, resulting in a face-on arrangement of Zn-P_6. (c) Edge-on assembly of Zn-P_{12} bridged by 4,4′-bipyridine.

an optimal fashion [57]. It was estimated that the adsorption free-energy for RhCl-T(C_{18}OP)P·Py is 5.1 kJ mol^{-1} less than that of H_2-T(C_{18}OP)P. Preparation of an ordered array was made possible either by mixing with the free-base porphyrin molecules with the same hydrocarbon chain length or using Rh-porphyrin with longer hydrocarbon chains, e.g., RhCl-T(C_{30}OP)P·Py. Fig. 10 shows the assembly of a mixture of RhCl-T(C_{18}OP)P complexed with 4-phenylazopyridine and H_2-T(C_{18}OP)P at the 1-phenyloctane/HOPG interface. The brighter spots with the higher profile corresponds to RhCl-T(C_{18}OP)P·(4-phenylazopyridine) molecules.

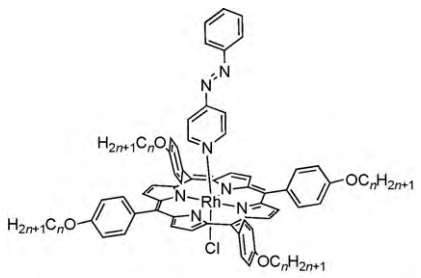

RhCl-T(C_{18}OP)P·(4-phenylazopyridine)

Labile axial coordination to Zn-porphyrins was probed with STM at the 1-phenyloctane/HOPG interface [58]. The spots in STM images for the complex, Zn-T(C_{18}OPP)·(4-phenylazopyridine), appeared distinctly higher than H_2-T(C_{18}OP)P as shown in Fig. 11 or ligand-free Zn-T(C_{18}OP)P. Interestingly, the complexes with *trans*-4-phenylazopyridine appear higher than those with a mixture of *trans*/*cis*-4-phenylazopyridine. We can deduce two things from this observation. One is that STM can distinguish *trans* and *cis* configurations of a molecule that is "standing" on the surface. The second is that the association/dissociation rates for the axial coordination are faster than the STM time scale so that a kind of average height is recorded for the *tans*/*cis* mixture, instead of two distinct heights.

Similar systems using Zn-TC_{12}P, in which alkyl groups are directly attached to the *meso* position of the porphyrin macrocycle, in place of Zn-T(C_nOP)P were investigated for axial coordination [59]. Ordered arrays of Zn-TC_{12}P are obtained on the surface of HOPG, as described earlier. On addition of 3-nitropyridine as an axial ligand, some spots appear higher than the rest of porphyrin molecules. The higher and the lower spots were assigned to the ligated and ligand-free porphyrin molecules, respectively. This is rather surprising because this means that the rate of association/dissociation of 3-nitropyridine and Zn-TC_{12}P is slower than the time scale of STM, which is in contrast to the case for Zn-T(C_nOP)P described above. Another interesting observation for this system is that the binding between the axial ligand and the Zn-porphyrin is much enhanced than that in solution. These two results are most likely due to the direct adsorption of the porphyrin plane to the surface of HOPG. Conformational and electronic changes are

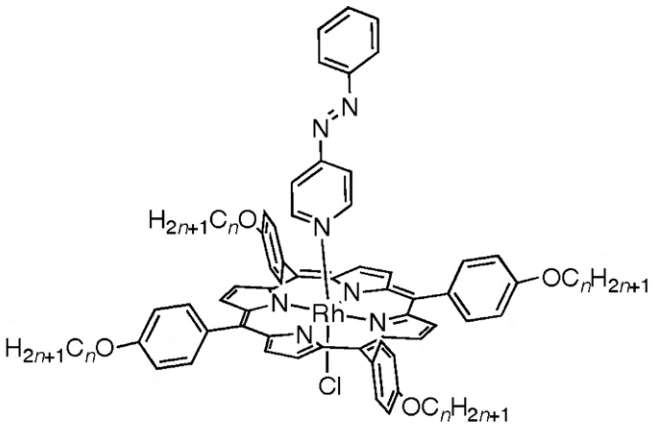

RhCl-T(C_{18}OP)P·(4-phenylazopyridine)

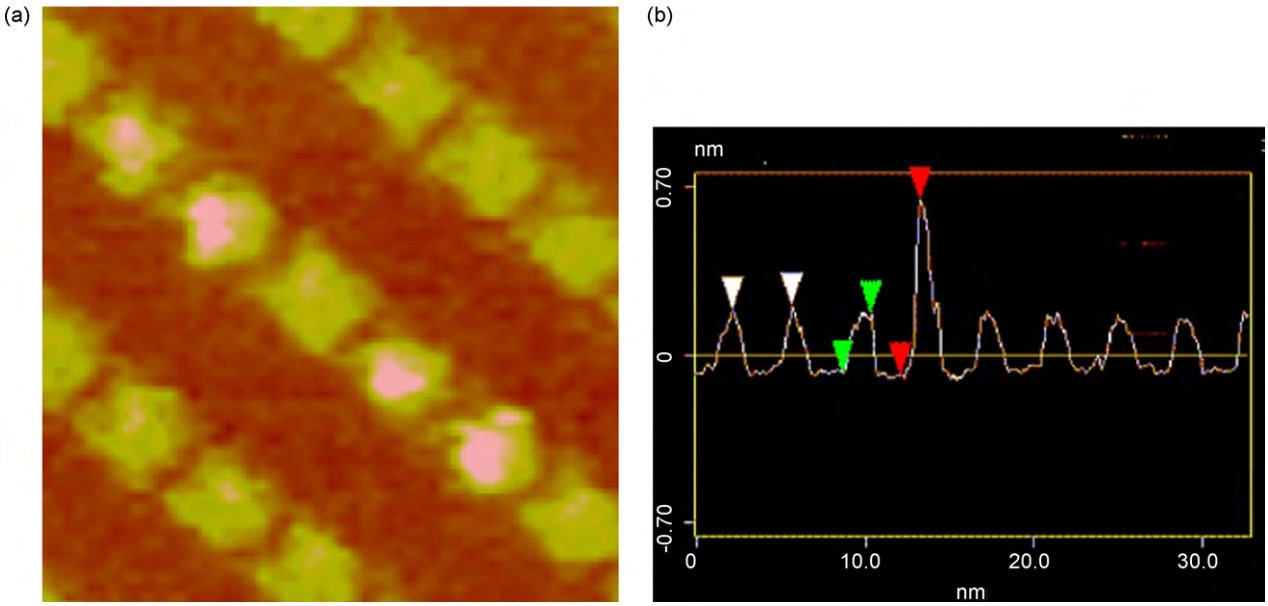

Fig. 10. STM for a mixed array of RhCl-T(C_{18}OP)P·(4-phenylazopyridine) and H_2-T(C_{18}OP)P at the 1-phenyloctane/HOPG interface. (a) STM image, 10 nm × 10 nm. (b) Height profile.

brought about by strong interactions of the porphyrin macrocycle with the HOPG surface. Thus, the surface adsorption may have dramatic consequences on the kinetics and thermodynamics of the axial coordination.

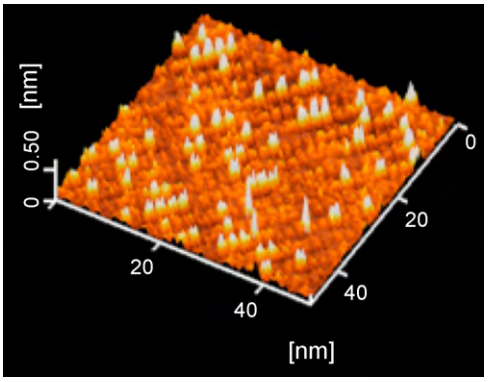

Fig. 11. STM for Zn-T(C_{18}OP)P·(4-phenylazopyridine) (higher spots) and H_2-T(C_{18}OP)P (lower spots) at the 1-phenyloctane/HOPG interface. Reproduced with permission from Ref. [58].

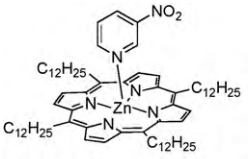

Zn-TC_{12}P·(3-nitropyridine)

2.6. STM with chemically modified tips

Specific interactions, such as hydrogen bonding, coordination and charge transfer interactions, may enhance the tunnel current. This enhancement was demonstrated using chemically modified tips (Fig. 12). While Zn-, Ni-, and free-base porphyrins cannot be discriminated using Au tips, Zn-porphyrin appears brightest with 4-mercaptopyridine modified tips [60]. The specificity for the Zn-porphyrin was attributed to the pyridine–zinc coordination interactions. Zn-porphyrin is also discriminated from free-base porphyrin with a C_{60}-modified tip [61]. It is proposed that the charge transfer interactions, in which a negative charge is transferred from the Zn-porphyrin molecules adsorbed on the surface to the C_{60} moiety on the tip, are responsible for the discrimi-

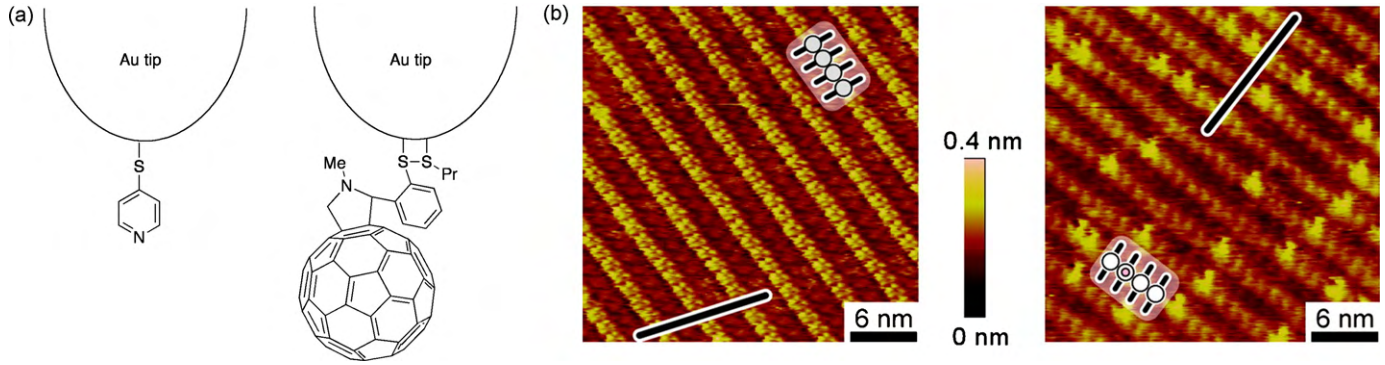

Fig. 12. STM with chemically modified STM tips. (a) Chemical structures [60,61]. (b) STM images of mixed monolayers of free-base porphyrin and Zn-porphyrin physisorbed onto HOPG. (Left) Free-base and Zn-porphyrins are not distinguishable with an unmodified gold tip. (Right) Zn-porphyrins are observed brighter with a C_{60}-modified tip. Reproduced from Ref. [61]. Copyright (2005) National Academy of Sciences, U.S.A.

nating ability. The HOMO level of the Zn-porphyrin (−5.4 eV) is higher than that of the free-base porphyrin (−5.7 eV) and hence the charge transfer to the LUMO of the C_{60} (−4.1 eV) from the Zn-porphyrin is more facile at low bias potentials. Interestingly, the *I–V* curve obtained on a porphyrin molecule with the C_{60}-modified tip showed a rectifying behavior. More electrons flow in the direction from the porphyrin on the substrate to the C_{60} on the tip, in accordance with the direction of the charge transfer interaction.

3. Porphyrin assemblies at metal/electrolyte interfaces: EC-STM studies

3.1. Single component assemblies at metal/electrolyte interfaces

The interface of a substrate and an electrolyte solution is an attractive target for STM studies because the interface has a relevance to various electrochemical reactions. Furthermore, in EC-STM, the substrate potential can be controlled independently from the tip–substrate bias voltage. This gives an additional parameter that can be used to control not only the surface redox state but also the structure of the assembly.

Only disordered adlayers of water-soluble H_2-T(MPy)P tetracation are formed on the Au(1 1 1) surface because the mobility of the molecules is too low to rearrange themselves into any ordered array [62]. Well-ordered arrays of this and other molecules form on an iodine-modified Au(1 1 1) surface (I–Au(1 1 1)) [62,63], I–Ag(1 1 1) [64], I–Pt(1 0 0) [65], as well as on sulfur-modified Au(1 1 1) (S–Au(1 1 1)) [66], which were successfully observed at submolecular resolutions in electrolyte solutions with EC-STM. The iodine or sulfur adlayer lowers the interactions of the molecules with the substrate, allowing them to diffuse on the surface until being incorporated in an ordered array. The iodine-modified Au(1 1 1) surface, i.e., an iodine monolayer adsorbed on the Au(1 1 1) surface, was prepared by immersing the Au(1 1 1) substrate into a KI solution for a few minutes followed by thorough rinsing. The sulfur-modified Au(1 1 1) surface was likewise prepared by immersing the substrate into a Na_2S solution under a constant potential condition.

Alternative method for modulating the diffusivity of molecules on surfaces can be achieved through the adjustment of the substrate potential in the EC-STM. STM studies for the self-assembly of H_2-TPyP revealed that at positive potentials >0.5 V vs. SCE, disordered molecules are immobile on the surface [67]. However, at negative potentials <−0.2 V vs. SCE, the molecules are highly mobile. At intermediate potentials −0.2 to +0.2 V vs. SCE, the molecules formed a highly ordered adlayer. The series of experiments demonstrated that the two-dimensional diffusion barrier is important for the formation of ordered adlayer and that the diffusion barrier can be modulated by changing the substrate potential in the EC-STM.

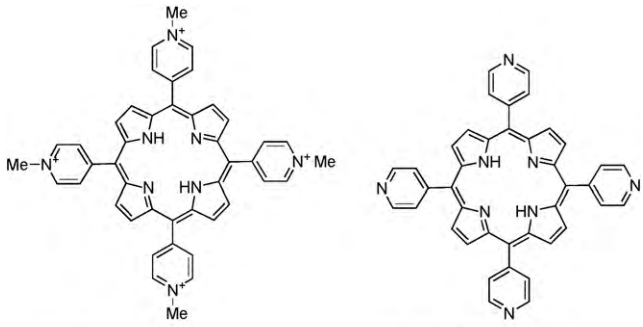

H_2-T(MPy)P H_2-TPyP

Monolayers of water-insoluble porphyrins and phthalocyanines were prepared by immersing a substrate into a benzene solution of the molecule of interest. While porphyrin molecules, Co-TPP [68], Cu-TPP [68], and Co-OEP [69], induce the reconstruction of the Au(1 1 1) to the ($\sqrt{3} \times 22$) phase upon adsorption, forming well-ordered adlayers, cobalt(II) porphine (Co-P) [69] without any substituents on the porphyrin macrocycle forms well-ordered arrays on the Au(1 1 1) surface but without inducing the reconstruction. Adsorption-induced reconstruction or lifting of reconstruction depending on the molecule are also observed for the Au(1 0 0) surface. Cu-TPP and Co-TPP induce the reconstruction to the Au(1 0 0)-(hex), while Co-Pc causes the lifting of the reconstruction [70].

Surface assemblies and O_2 adduct formation of a cobalt(II) "picket-fence" porphyrin, Co-T(pivP)P, were investigated on Au(1 1 1) and Au(1 0 0) in 0.1 M $HClO_4$ solutions [71]. The molecules adsorb on the surfaces with the pivalamide (Bu^tCONH–) group pointing away from the surface. The molecules form well-ordered arrays both on Au(1 1 1) and Au(1 0 0)-(hex) surfaces. There is a preferred orientation for the growth of the ordered domain, resulting in the formation of belt-like long domains tens of nanometers wide. Under an O_2 atmosphere, O_2 adduct formation is observed as bright spots on the porphyrin on the Au(1 0 0)-(hex) surface. The adduct formation, however, is not observed on the Au(1 1 1) surface. These observations suggest that the arrangement of Au atoms underlying the molecule has a decisive influence on the coordination of O_2 to the cobalt atom.

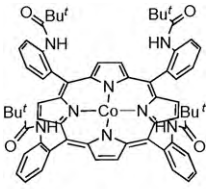

Co-T(pivP)P

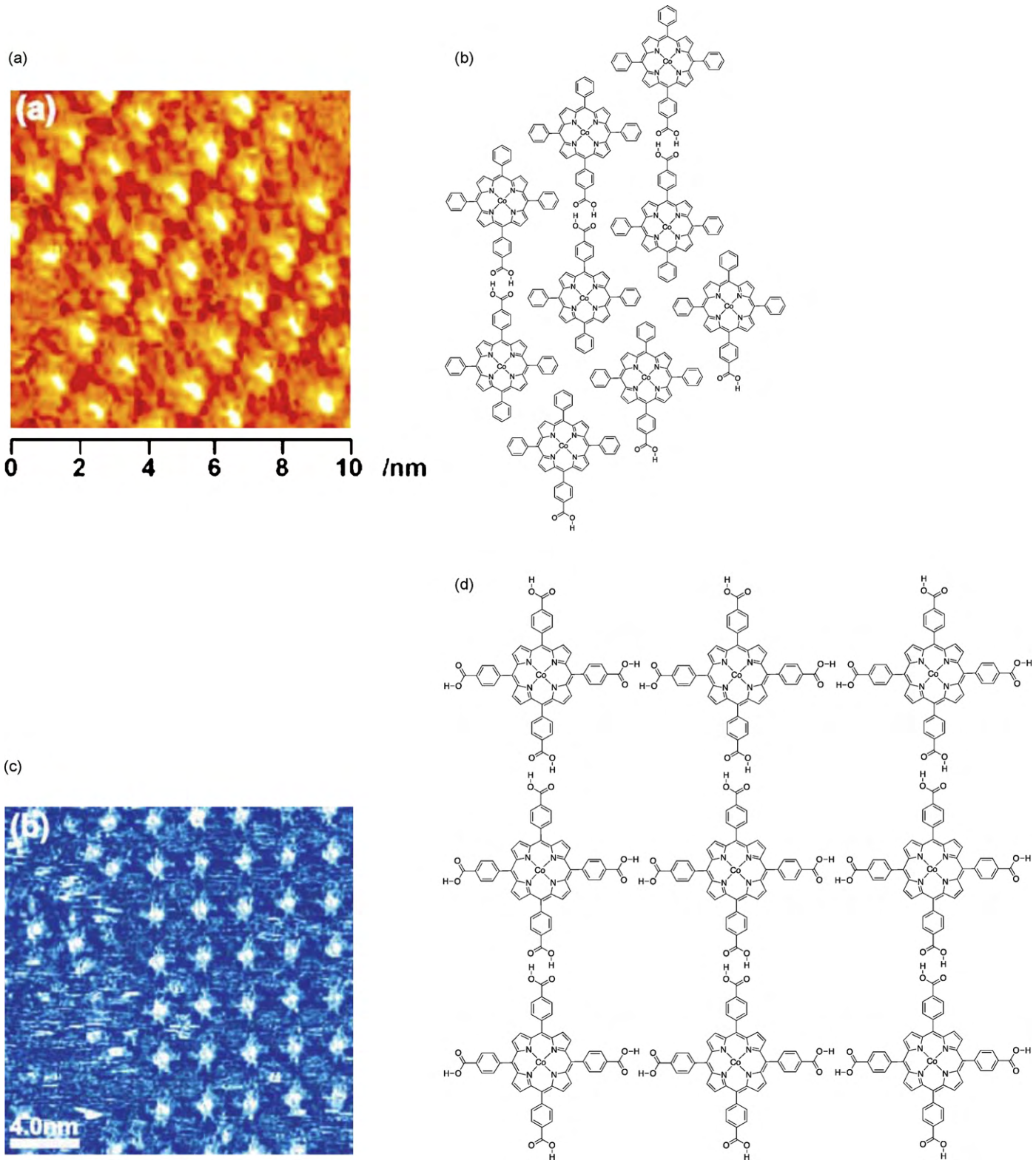

Fig. 13. Assemblies of porphyrins with carboxylic acid groups. (a and b) Co-(HO_2CP)P_3P. (c and d) Co-T(HO_2CP)P. Reproduced with permission from Ref. [72].

Directional intermolecular interactions have been utilized to prepare tailor-made surface patterns at metal/electrolyte interfaces. Porphyrins with carboxylic acid functionalities were investigated for this purpose. Thus, the porphyrin with one carboxyl group on a *meso*-phenyl group, Co-(HO_2CP)P_3P, assembles into a dimer, which then form well-ordered arrays to fill the surface as shown in Fig. 13a [72]. The porphyrin with four carboxyl groups on the *meso*-phenyl groups, Co-T(HO_2CP)P, assembles into an infinitely extending grid-like structure with large cavities as shown in Fig. 13b. In both cases, the assembly formation is directed by the complementary hydrogen bonding of a pair of carboxylic acid moieties. Order–disorder transitions can be induced for these assemblies by modulating substrate potential under the electrochemical environment.

Adlayer structures of triple-decker complex, (TPP)Eu(Pc-15C5)Eu(Pc-15C5), were investigated on the Au(1 1 1) surface at the electrochemical interface [73]. The triple-decker complexes were deposited from a benzene solution. Well-ordered domains formed under appropriate preparation conditions, in which two types of features are arranged in a chessboard pattern. The two types of features were assigned as complexes oriented with the TPP ligand upward and the Pc-15C5 ligand upward. The orientation can be controlled by modulating the substrate potential. The adlayer shows partly reversible redox couple around 0.2 V vs. RHE in 0.05 M $HClO_4$. The analysis of the STM images suggested that the molecules with a topmost TPP ligand are reversed at potentials less than this redox couple, where the molecule is one-electron oxidized.

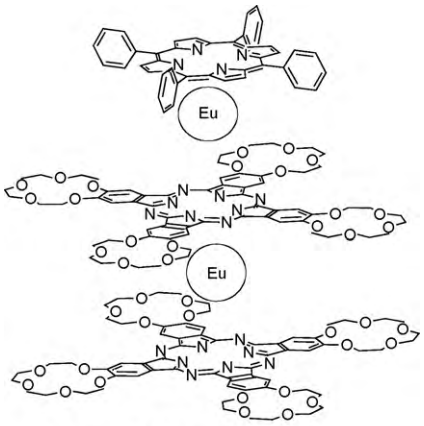

(TPP)Eu(Pc-15C5)Eu(Pc-15C5)

3.2. Multicomponent assemblies at metal/electrolyte interfaces

Studies of multicomponent surface assemblies should lay the foundation for the development of increasingly complex architectures. Specific intermolecular interaction sites must be incorporated into the structures of component molecules to obtain well-defined heterotopic assemblies. Analysis of resulting supramolecular structures and dynamics may help to obtain insight into intermolecular interactions that play a role at the two-dimensional surfaces.

A binary mixture of Co-Pc and Cu-TPP on Au(1 1 1) in 0.1 M $HClO_4$ gives several domains [74]. A part of the surface is covered by well-ordered arrays of Cu-TPP, while the other part is covered by disordered Co-Pc and Cu-TPP molecules. On the contrary, highly ordered alternate rows of Co-Pc and Cu-TPP are observed on Au(1 0 0).

Zn-OEP and Zn-Pc also form assemblies on the Au(1 1 1) surface with domains in which the arrangements are different [75]. A major pattern is a "chessboard" consisting of Zn-Pc and Zn-OEP "squares". Another pattern consists of alternate rows of Zn-Pc and Zn-OEP, with each of the rows being straight or zigzag, depending on the location on the substrate and applied substrate potential. This binary mixture also forms ordered arrays on the Au(1 0 0)-(hex) surface, which consist of separate rows of Zn-OEP and Zn-Pc molecules. The combination of Zn-TPP and Zn-OEP produces a nanohexagonal pattern on the Au(1 1 1) surface, in which Zn-OEP molecules, each surrounded by eight Zn-TPP molecules, are arranged in a hexagonal lattice.

The substrate potential provides a means to control the structure of the surface two-dimensional arrays. For mixtures of Cu-OEP and Co-Pc on Au(1 1 1), supramolecular structures transform depending on the substrate potential [76].

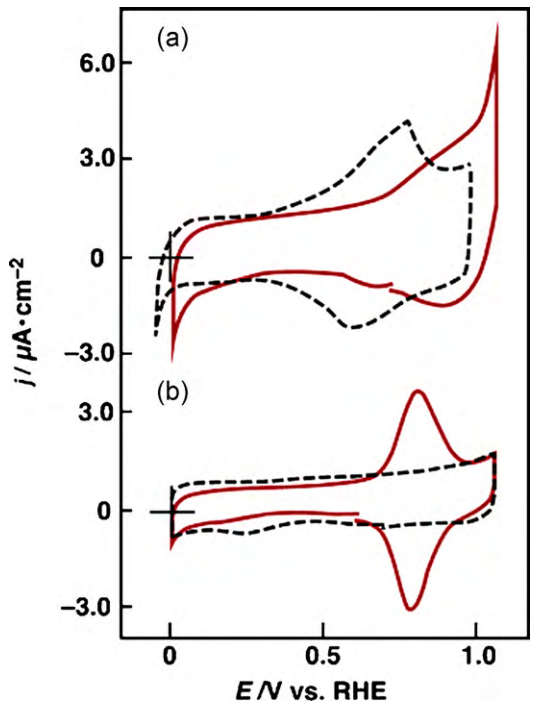

Fig. 14. Cyclic voltammograms of (a) bare Au(1 1 1) (dotted line) and C_{60}Fc-adsorbed Au(1 1 1) (red solid line) and (b) Zn-OEP adsorbed (dotted line) and Zn-OEP·C_{60}Fc-adsorbed (red solid line) Au(1 1 1) electrodes in 0.1 M $HClO_4$. Reproduced with permission from Ref. [78].

A superstructure of 1:1 complexes of Zn-OEP and C_{60} was prepared on the Au(1 1 1) surface [77]. The Zn-OEP molecules adsorb to the Au(1 1 1) surface to form close-packed arrays with an intermolecular distances of 1.40 and 1.65 nm. C_{60} molecules alone also adsorb on the Au(1 1 1) surface, affording a close-packed hexagonal structure with the center-to-center intermolecular distance of 1.0 nm. When a Au(1 1 1) substrate was successively immersed into a benzene solution of Zn-OEP and a benzene solution of C_{60}, STM data acquired in an electrolyte solution revealed that the array of C_{60} exhibits the identical lattice structure with that of Zn-OEP. This observation indicates that the C_{60} molecule is placed on top of each of the Zn-OEP molecules, forming supramolecule, Zn-OEP·C_{60}.

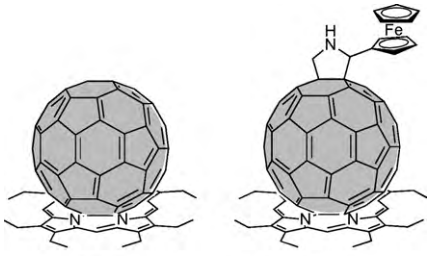

Zn-OEP·C_{60} M-OEP·C_{60}Fc

A ferrocene derivative of C_{60}, C_{60}Fc, directly attached to the Au(1 1 1) surface showed only poorly defined electrochemical redox response. However, a clear electrochemical redox reaction of the ferrocene group in the C_{60}Fc molecule was observed at 0.78 V vs. RHE on Zn-OEP, Co-OEP, and Cu-OEP adlayers as shown in Fig. 14 [78]. The well-defined redox wave is attributed to the well-defined orientation of the C_{60}Fc molecules bound to the M-OEP molecules. This is a good example of supramolecular species giving a better-defined structure and function therefrom than the component molecules. Whereas the Zn, Co, Cu complexes of OEP give identical results, FeCl-OEP does not give a well-defined structure nor a well-defined redox reaction. Apparently, the chloride

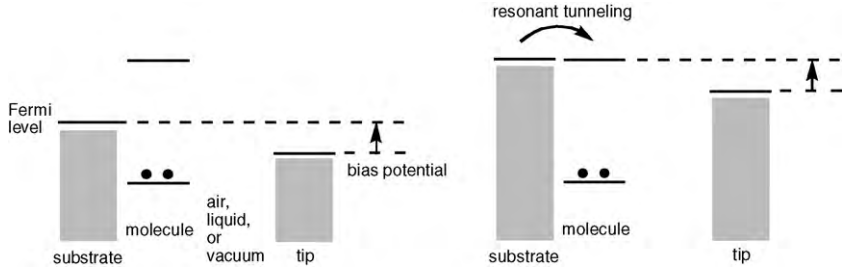

Fig. 15. In the EC-STM, the substrate potential can be controlled independently from the bias potential. (Left) The substrate potential is in the middle of the HOMO and LUMO of the adsorbed molecule and off-resonant from the molecular orbital levels. (Right) The substrate potential is negatively shifted so that it is on-resonant with the LUMO of the molecule. The electric current can now flow via a "resonant tunneling" process. Note that the bias voltages are common to both cases.

ion coordinated to the central Fe ion prevents the supramolecular complex formation between the porphyrin and the C_{60}Fc molecule.

C_{60} molecules are also immobilized on the chessboard arrangement of Zn-OEP and Zn-Pc on Au(1 1 1). At low coverage, the C_{60} molecules are located in the gaps surrounded by Zn-OEP and Zn-Pc molecules [75]. It is implied that an increased charge density of the gap sites of the gold surface due to the adsorption of Zn-OEP and Zn-Pc molecules drives the adsorption of C_{60} on the sites. This adsorption site is different from that for the pure Zn-OEP arrays, in which case C_{60} adsorbs right on top of the porphyrin molecule. With increasing coverage, the C_{60} molecules are deposited on the Zn-Pc molecules with centers somewhat offset. No ordered assembly of C_{60} molecules was observed on the mixed arrays of Zn-OEP and Zn-Pc on the Au(1 0 0)-(hex) surface. The assembly of C_{60} molecules is strongly influenced by the bimolecular packing arrangement of Zn-OEP and Zn-Pc, which depends on the crystallographic orientation of the substrate.

3.3. Electronic processes in EC-STM

In the EC-STM, the substrate potential can be controlled with respect to molecular redox potentials independent of the bias potential (Fig. 15). Thus, the redox state of the adsorbed molecule can be controlled with the substrate potential, while the imaging is performed with independently adjustable bias potentials with respect to the tip potential.

An early demonstration of resonant tunneling was reported for a mixed array of iron(III) protoporphyrin IX and free-base protoporphyrin IX. With the substrate potential at −0.4 V vs. SCE, where the LUMO of ion(III) protoporphyrin IX is in resonance but that of the free-base counterpart is not, the ion(III) protoporphyrin IX appears much higher than the free-base counterpart [79].

Electron transfer reactions at the electrode–electrolyte interface have been studied at the molecular level by EC-STM [80]. A well-ordered two-dimensional monolayer assembly of H_2-TPyP was prepared on the Au(1 1 1)/0.1 M H_2SO_4 interface. The substrate with the monolayer was initially held at −0.1 V vs. SCE, where all the H_2-TPyP molecules were reduced. A short (0.1–1 s) pulse of the oxidation potential (0.2–0.3 V vs. SCE) was applied to the sample during STM imaging. STM can distinguish oxidized porphyrin molecules, which appear darker, from reduced porphyrin molecules. Hence the redox reaction can be monitored for each molecule. Observation of individual molecules revealed that the oxidation occurs not randomly but patchwise under certain conditions. Interestingly enough, the locations of individual oxidized H_2-TPyP molecules change within the ordered array, which is indicative of hole hopping diffusion in the two-dimensional assembly.

4. Porphyrin assemblies on metal surfaces: UHV-STM studies

4.1. Conformations of porphyrins adsorbed on metal surfaces

Molecular adlayers on a metal substrate may form upon sublimation of the molecules under UHV conditions. Probably the best characterized porphyrin molecule with UHV-STM is M-T(DBP)Ps (Table 1). In general, the conformation of adsorbed molecules on surfaces is important because it determines the properties of the molecules as well as electronic interactions between the molecule and the substrate. Particularly for metalloporphyrins such as M-T(DBP)P, the distance between the central metal ion and the substrate surface is critically dependent on the twist angle of the phenyl groups and the distortion of the porphyrin macrocycle. Thus, the interactions and electronic coupling of the metal in the macrocycle and the surface is determined by the molecular conformation.

Table 1
Arrangements and conformations of T(DBP)Ps.

Porphyrin	Surface	Arrangement	θ	ϕ	Refs.
Co-T(DBP)P	Ag(1 1 1)	Square	90°	25°	[81]
	Ag(1 1 1)	Hexagonal	60°	45°	[81]
	Ag(1 1 1)	Hexagonal	45°	15°	[81]
	Ag(1 1 1)	Herringbone	20°	5°	[81]
Zn-T(DBP)P	Ag(1 0 0)		90°		[82]
Pt-T(DBP)P	Cu(1 0 0)	Square			[83]
Cu-T(DBP)P	Cu(1 0 0)		67°–83°		[84]
	Cu(1 0 0)	Square	90°		[85]
	Au(1 1 0)	Rectangular	45°		[85]
	Ag(1 1 0)	Rectangular	30°		[85]
	Cu(1 1 1)	Herringbone			[86]
	Cu(2 1 1)		10°, 55°		[87]
H_2-T(DBP)P	Au(1 1 1)	Hexagonal			[88]
	Au(1 1 1)	Hexagonal	20°		[89]

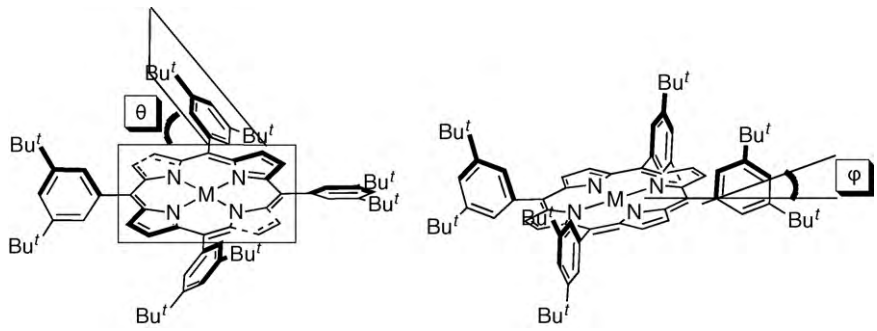

Fig. 16. Conformational variations of M-T(DBP)P molecules on surfaces [81]. θ and ϕ represent the twist and tilt angles, respectively.

The major factor for the conformational variation is the rotation of the four single bonds between the *meso*-carbons and phenyl-carbons defined by dihedral (twist) angle θ. For molecules in vacuum or in solution, this angle is determined as a compromise between planarization for maximum delocalization of the π electronic system and steric repulsion of the phenyl groups and the porphyrin periphery. For molecules adsorbed on a surface, interaction with the surface comes into play. For small θ values, distortion of the porphyrin macrocycle is induced by steric repulsion as shown in Fig. 16. Additional distortion is due to the tilt of the phenyl groups with respected to the porphyrin macrocycle as represented by ϕ.

Submolecular resolution of STM images makes it possible to distinguish these subtle conformational variations. For a rough estimation of the twist and tile angles, an assumption is made that the topmost *t*-butyl groups appear highest in the STM image. This is a reasonable assumption considering that the STM samples spatial distribution of electron densities. Thus, depending on the twist angles, the arrangement of the four brightest spots varies from a square to a rectangle as shown in Fig. 17. For molecules with small twist angles, a dark line appears through the center of the porphyrin in parallel with the longer sides of the rectangle. This orientation of the dark line is consistent with assumed molecular conformation as the orientation agrees with the depressed pyrrole rings caused by the steric hindrance by the phenyl rings.

The conformations of Cu-T(DBP)P were characterized on single-crystal metal surfaces including Cu(1 0 0), Au(1 1 0), and Ag(1 1 0) [85]. Four dots arranged in a square were observed for the molecules on the Cu(1 0 0) surface. Hence, the dihedral angle of 90° was estimated. On Au(1 1 0), the dihedral angle of 65° in a mobile precursor state changes into that of 45° after extended annealing accompanying the formation of a well-ordered assembly.

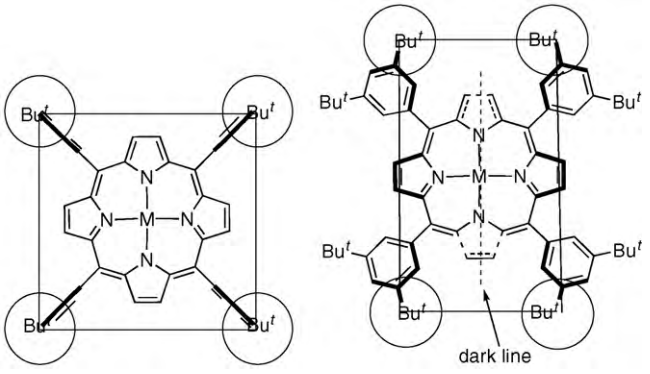

Fig. 17. Correspondence of STM images to the molecular conformation of M-T(DBP)P. Encircled *t*-butyl groups appear as the highest spots in the STM topography. A square arrangement is observed for the dihedral angel $\theta = 90°$, which becomes rectangular as the angle is decreased.

For Co-T(DBP)P sublimed on the Ag(1 1 1) surface, four different molecular arrangement were found [81]. Upon sublimation to a coverage less than one monolayer, three distinguishable molecular arrangement were found: one square and two different hexagonal arrangements. On the other hand, deposition of a multilayer followed by annealing to desorb the excess molecules lead to a herringbone arrangement. The conformations of the 3,5-di-t-butylphenyl groups with respect to the porphyrin plane are associated to specific arrangements. In addition to the twist angles, the tilt angles, as shown in Fig. 16, have also been analyzed.

For the free-base counterpart, H_2-T(DBP)P, adsorbed on Au(1 1 1), a distorted conformation was revealed with STM [89]. Comparison with a molecular model showed that the twist angle at 20° is consistent with the STM studies.

A prototype of molecular switch is proposed on the basis of conformational manipulation. The twist angle in Cu-T(DBP)P on Cu(2 1 1) can take values of either 10° or 55° [87]. The phenyl group is virtually flat in the former case while it is rotated out of the plane in the latter case. As the tunneling resistance is larger in the former than in the latter, these two states can be regarded as an off state and an on state, respectively. The on state and the off state are reversibly controlled by manipulation with the STM tip. Lateral manipulation of the porphyrin molecule induces a rotation of the legs out and/or in the porphyrin plane. Vertical manipulation reorients the leg from the rotated to the flat conformation. In a demonstration of the switching behavior, the porphyrin molecule was initially in the on state and the tip was placed at a distance (Fig. 18). A current of $\sim 3 \times 10^{-9}$ A was recorded. As the tip was brought closer to the sample, the current increases to reach a plateau, where the phenyl ring was in transition from the rotated to the flat orientation. Then an abrupt increase in current followed by a plateau was observed, where the flat orientation, i.e., the off state, was reached. The molecule was in the off state throughout the retracting process. At the time the tip returned to the original position, a current of 1×10^{-9} A was recorded. It means that a bistability was realized. The energy required to operate this switch was determined

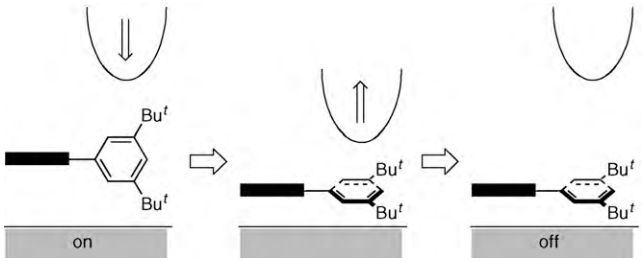

Fig. 18. Schematic illustration of a single molecule switch by means of the manipulation of the Cu-T(DBP)P conformation with an STM tip [87].

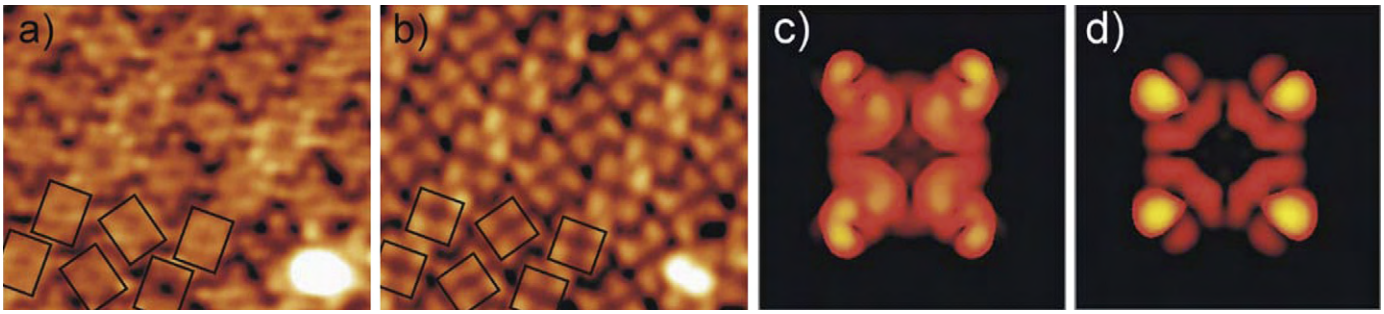

Fig. 19. Voltage-dependent images of H_2-TPyP on Ag(1 1 1). STM images with $V_{sample} = -0.9$ V and $I = 0.65$ nA (a) and that with $V_{sample} = 1.6$ V, $I = 0.65$ nA (b). The nearest neighbor intermolecular distance is 1.39 nm. A constant electron density contour obtained by integration over occupied states (c) and unoccupied states (d). Reproduced with permission from Ref. [91].

as less than 100×10^{-21} J with atomic force microscopy [90]. It was pointed out that this energy is 4 orders of magnitude lower than state-of-the-art transistors.

The STM gives different images for H_2-TPyP on Ag(1 1 1) depending on the bias voltage [91]. At negative sample bias voltages, the envelope of the molecule appeared as a rectangle (Fig. 19a), while at positive sample bias voltages, molecular shape is close to a square (Fig. 19b). These bias dependent images are consistent with calculated molecular orbitals. A constant electron density contours were made by integrating over relevant molecular orbitals. The contours were obtained as a function of the twist angle of the phenyl groups with respect to the porphyrin mean plane. The analysis indicated that the twist angle around 60° best explains the observed shape of the STM images.

A constant electron density contour made by integrating over the HOMO to HOMO−6 is shown in Fig. 19c. There is some intensity in the core and the legs have roughly the same apparent height arranged in a rectangle. Likewise, the electron density contour made by integrating over the LUMO to LUMO+4 is shown in Fig. 19d. The obtained contour diagram shows four bright spots arranged in a square with a hole at the center. These calculated images are quite consistent with the experimentally observed STM images, supporting the estimated value for the twist angle.

Both hexagonally packed domains and quasi-square packed domains are possible for H_2-T(DBHOP)P on Cu(1 1 1) (Fig. 20) [92,93]. For the molecules in the hexagonal domain, the dihedral angle between the porphyrin plane and the phenyl plane is estimated to be 10–20°, while for those in the quasi-square domains, the dihedral angles are ∼45° in alternate senses. Interestingly, these two phases can coexist in contact without any disorder. This is made possible by the existence of molecules at the interface of these domains, which take a mixed conformation. In the mixed conformation, the dihedral angle is ∼45° on the side of the quasi-square domain, while it is 10–20° on the side of the hexagonal domain. Thus, the buffer layer made of a single molecular chain makes the transition smooth between the two different arrangements.

Oxidation of H_2-T(DBOHP)P into the quinoid type compound has a dramatic influence on the conformation [94]. The *meso*-phenyl groups are now almost coplanar with the macrocyclic least squares plane. The planarization is a manifestation of the delocalization of the π electronic system over the phenyl and porphyrin moieties. Due to the severe steric repulsion between the pyrrole β hydrogen atoms and the phenyl ortho hydrogen atoms, the pyrrole rings are rotated away from the porphyrin plane by ±48° in an alternating fashion. The planar phenyl groups is deposited parallel to the surface when adsorbed. The oxidized H_2-T(DBHOP)P-ox

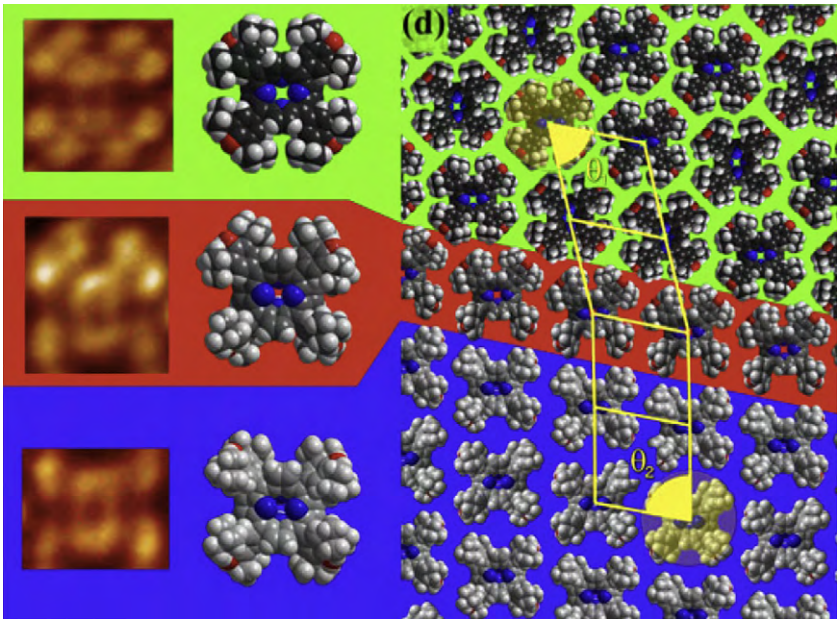

Fig. 20. Boundary region of two different surface assemblies of H_2-T(DBHOP)P [92,93]. Top domain: hexagonal phase where porphyrin molecules are in a relatively flat conformation with the tetrapyrrole/phenyl dihedral angle of 10–20°. Middle domain: buffer layer where porphyrin molecules are in a mixed conformation. Bottom domain: quasi-square phase where porphyrin molecules are in twisted conformation with the tetrapyrrole/phenyl dihedral angle of ∼45°. Reproduced with permission from Ref. [92].

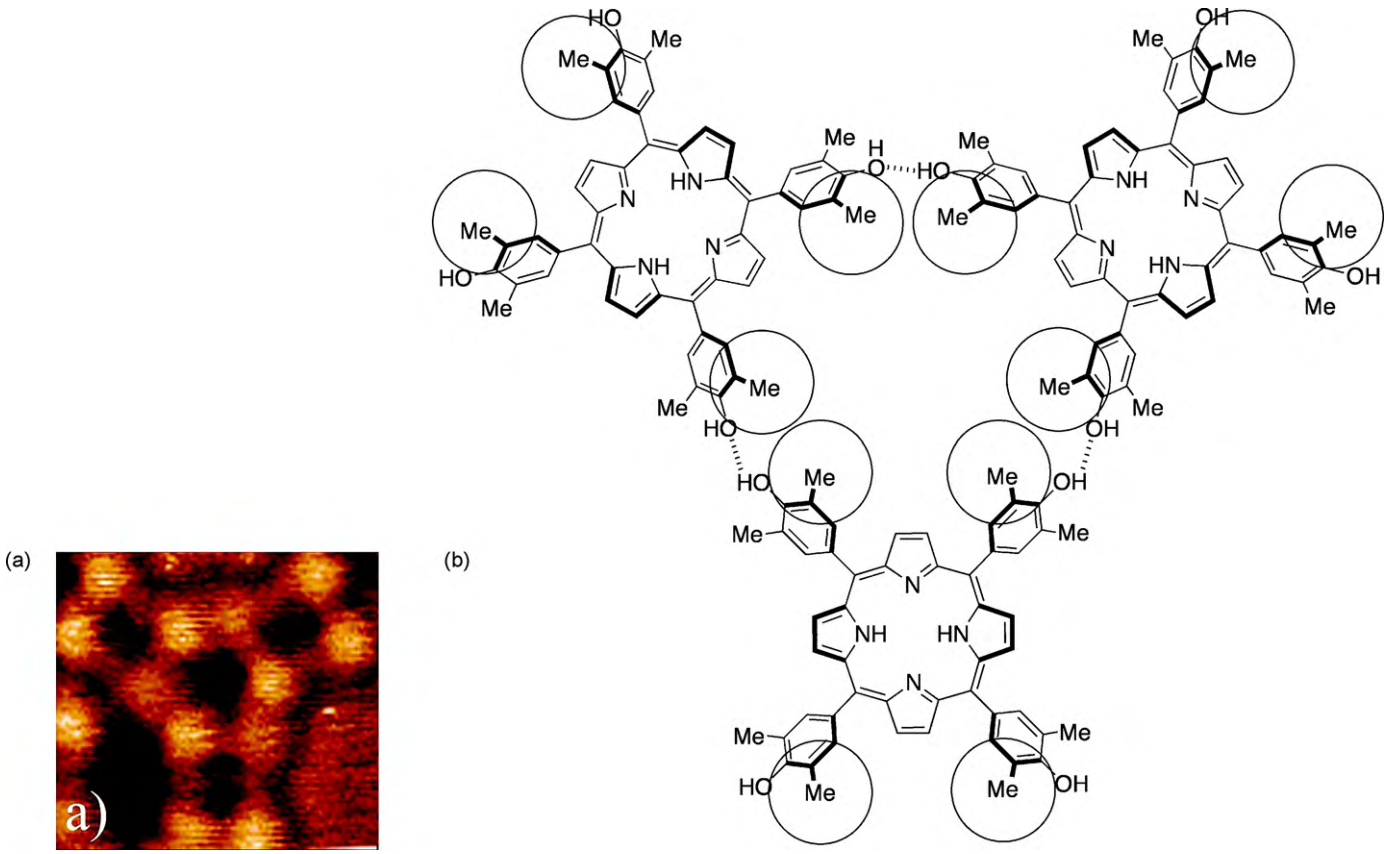

Fig. 21. One of the hydrogen-bonded trimeric units of H_2-T(DMHOP)P. (a) STM image. (b) Molecular structure. Reproduced with permission from Ref. [95].

molecules form only the hexagonal structure owing to the planarity of the phenyl groups.

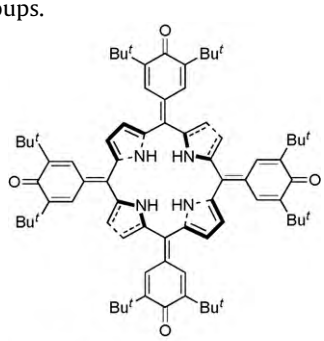

H_2-T(DBHOP)P-ox

For H_2-T(DBHOP)P, the *t*-butyl groups prevent the formation of hydrogen bond between the hydroxyl groups. Replacing the *t*-butyl groups by methyl groups make the hydrogen bonding possible. Thus, H_2-T(DMHOP)P molecules form hydrogen-bonded patterns based on cyclic trimeric units at submonolayer coverages as shown in Fig. 21 [95]. At monolayer coverage more densely packed patterns form but with another type of hydrogen bonding network.

4.2. Porphyrin assemblies governed by directional intermolecular interactions on metal surfaces

Introduction of sites for specific intermolecular interactions makes it possible to fabricate patterns on surfaces by self-assembly. An example has already been described in the previous section. An exemplary demonstration of this general principle was provided by the assembly structures of porphyrin molecules incorporating cyanophenyl groups in specific positions (Fig. 22) [96]. Formation of weak hydrogen bonds CH. . .NC among benzonitrile molecules is suggested from molecular orbital calculations. STM taken at 63 K for the porphyrin molecules containing one cyanophenyl group, H_2-(NCP)(DBP)$_3$P, adsorbed on Au(1 1 1) revealed that the molecules assemble into trimers. The porphyrin molecules containing two cyanophenyl groups at the *cis* positions, *cis*-H_2-(NCP)$_2$(DBP)$_2$P, assemble into tetrameric assemblies. The porphyrin molecules containing two cyanophenyl groups at the *trans* positions, *trans*-H_2-(NCP)$_2$(DBP)$_2$P form linear arrays. The weak CH. . .NC hydrogen bonds control the structures of the assembly.

Assemblies based on porphyrins bearing cyanophenyl groups have been further elaborated by using different derivatives including *trans*-Zn-(NCP)$_2$(DROP)$_2$P's [97] and *trans*- and *cis*-(NCPP)$_2$(DBP)$_2$P [98]. A study on the assemblies obtained from *cis*-(NCPP)$_2$(DBP)$_2$P on Cu(1 1 1) are especially informative because the comparison of the structures obtained from this molecule with those obtained from *cis*-(NCP)$_2$(DBP)$_2$P on Au(1 1 1) has revealed an important influence exerted by the substrate on the conformation of the adsorbate and the structure of the assembly [98]. As described just above, the molecules of *cis*-(NCP)$_2$(DBP)$_2$P exclusively form tetramers on the Au(1 1 1) substrate [96]. In sharp contrast, everything from dimeric to hexameric as well as chain-like structures are formed from *cis*-(NCPP)$_2$(DBP)$_2$P on the Cu(1 1 1) surface. Two major factors are suggested as the reasons behind the difference in their behavior. Firstly, interactions involving cyanophenyl groups (i.e., CH/N hydrogen bonding) are weak compared to, for example, classic hydrogen bonds involving more acidic O–H or N–H hydrogen bond donors, thus allowing more room for adaptation in the structural motif. Secondly, and more importantly, molecule–substrate interactions are stronger with Cu(1 1 1) than with Au(1 1 1), thus more than compensating unfavorable molecule–molecule interac-

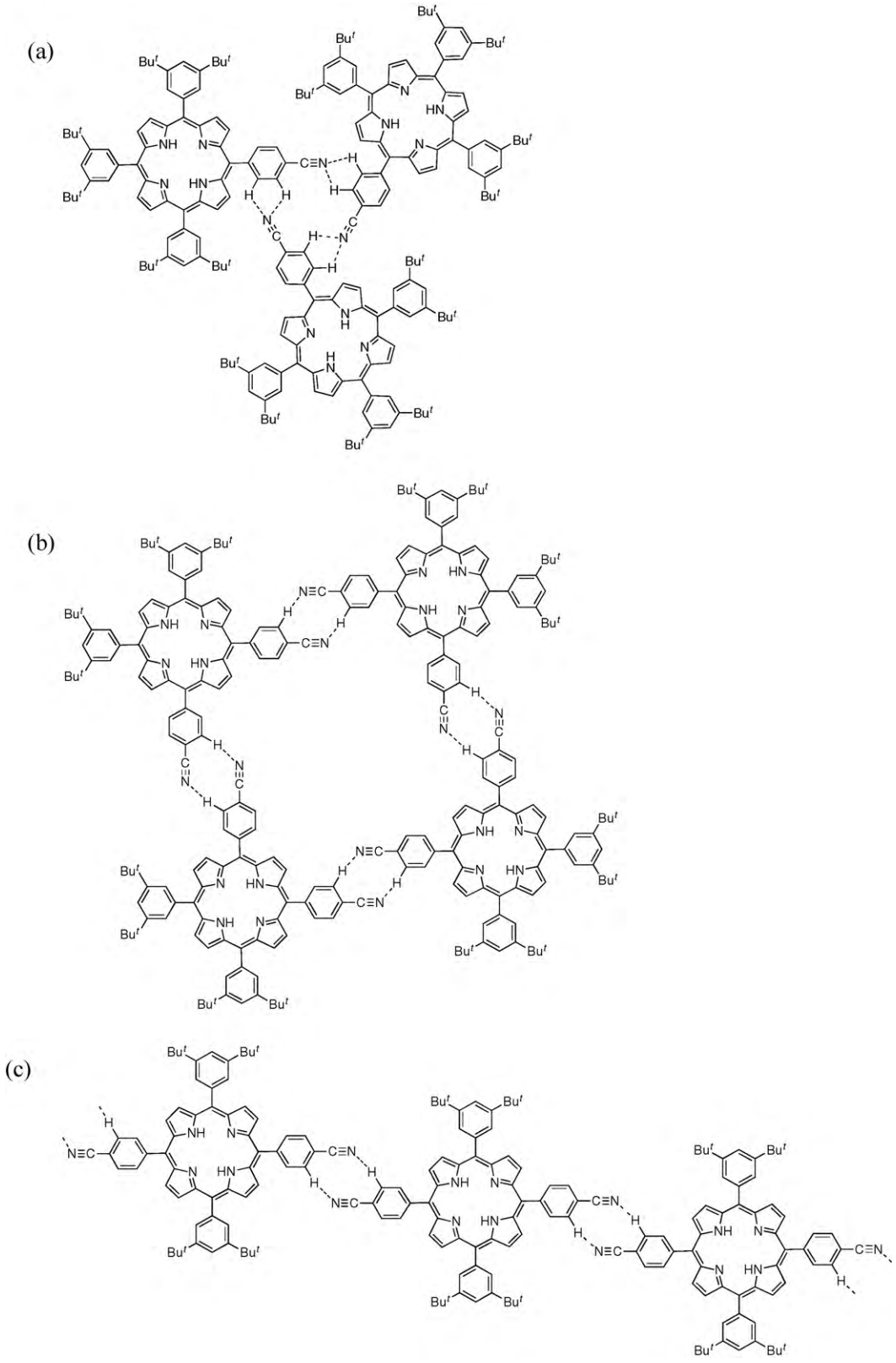

Fig. 22. Surface patterns formed from porphyrins bearing cyanophenyl groups. Dotted lines indicate hydrogen bonding as indicated by molecular orbital calculations. (a) H_2-(NCP)(DBP)$_3$P. (b) *cis*-H_2-(NCP)$_2$(DBP)$_2$P. (c) *trans*-H_2-(NCP)$_2$(DBP)$_2$P [96].

tions. The stronger interaction between the Cu(1 1 1) and adsorbed porphyrin molecules is manifested by the orientation of the dark lines appearing in the STM images of molecules, which represents the distortion of the porphyrin plane, as discussed above. In the case of the porphyrins on Au(1 1 1), the orientation of the dark lines are determined solely by the intermolecular interactions, whereas in the case of the porphyrins on Cu(1 1 1) the orientations of the dark lines are always in agreement with the Cu(1 1 1) main axes.

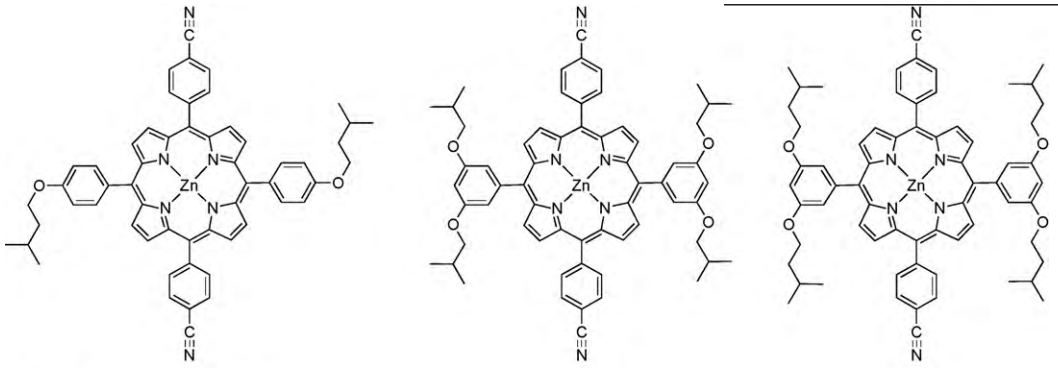

trans-Zn-$(NCP)_2(DROP)_2$P's

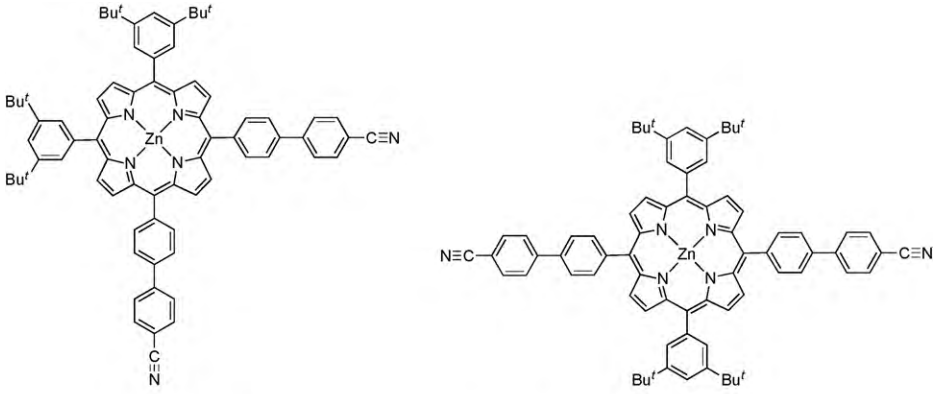

cis-$(NCPP)_2(DBP)_2$P *trans*-$(NCPP)_2(DBP)_2$P

Supramolecular surface assemblies arising from M-T(DBP)P derivatives bearing carboxyl groups on the Au(1 1 1) surface were also investigated [99]. The monocarboxylic acid derivative, H_2-$(HO_2CP)(DBP)_3$P, is chiral on the surface due to a saddle-like distortion induced by the adsorption. Upon adsorption of the molecule, the twist angle between the porphyrin mean plane and the phenyl plane reduces to ~20° from 60 to 90° in the ground state conformation. This change in the twist angle causes steric repulsion between the pyrrole β hydrogen atoms and the phenyl ortho hydrogen atoms, leading to the chiral saddle-like distortion. High-resolution STM images can distinguish the chirality by the appearance of a dark line across the porphyrin core. The monocarboxylic acid derivative forms a dimer unit on the surface through the formation of the optimal coplanar hydrogen bond between the carboxylic acid groups. The STM revealed that the chirality of the pairwise porphyrins are related as shown in Fig. 23a, resulting in an achiral assembly.

The relationship between the conformations or chirality of the hydrogen-bonded dimer applies to extended wire-like structure arising from the *trans*-dicarboxylic acid derivative, *trans*-H_2-$(HO_2CP)_2(DBP)_2$P. The orientation of the distortion alternates along the one-dimensional molecular chain to maintain the coplanarity between the hydrogen-bonded carboxyphenyl groups (Fig. 23c). The chains align side-by-side in the same direction to form bundles until most of the surface is covered as the coverage is increased. Upon further deposition of the molecules to a substrate covered by the monolayer of the bundle of chains, another layer of chains grow on the first layer chains along the same direction [100]. Layer-by-layer deposition experiments showed that the supramolecular wires are aligned with the underlying wires even in the fifth layer.

The *cis*-dicarboxylic acid derivative, *cis*-$(HO_2CP)_2(DBP)_2$P, forms a tetrameric units at low surface coverages, again through the formation of the optimal coplanar carboxylic acid dimers. The conformational analysis with high-resolution STM revealed that there are two conformational isomers on the surface, depending on the orientation of the distortion as shown in Fig. 23e. A tetrameric unit contains only either one of the conformers. At higher coverages, polymeric zigzag shaped one-dimensional chains form which then assemble into a bundle of chains. The conformation-selective association is maintained in the chains as well as in the bundles.

Just like hydrogen bonding, coordination interaction is a directional interaction that may be exploited in constructing well-defined supramolecular species on surfaces as well. Upon annealing of the samples of *cis*-$(NCPP)_2(DBP)_2$P on Cu(1 1 1), for which the formation of characteristic supramolecular patterns on sublimation is described earlier, at temperatures above 150 °C, dimeric macrocyclic structures are formed as schematically shown in Fig. 24 [98]. In this dimeric motif, it is proposed that the two porphyrins are bridged by Cu atoms. A number of Cu adatoms are provided from the step edges, which form coordination bonds with the cyanophenyl groups, giving rise to the dimeric structure.

Porphyrin substituted with 4-(pyrid-4-yl)ethynylphenyl groups in different numbers and in different positions were deposited on Cu(1 1 1) [101]. While these porphyrins for themselves do not feature an explicit structure directing group (without another hydrogen bond donor or metal ion), they still form well-defined supramolecular structures on deposition on the Cu(1 1 1) surface, in which the pyridyl groups are always oriented in near head-on configurations (Fig. 25). Coordination of the pyridyl groups to copper atoms is invoked to rationalize these supramolecular structures. Thus, the molecules of $(PyCCP)(DBP)_3$P, which bear a pyridyl group, form dumb-bell shaped dimers. In the case of *cis*-$(PyCCP)_2(DBP)_2$P, triangular and rhombic architectures consisting of three and four molecules are formed. Which of these assemblies dominate on the surface depends on the coverage. The trimeric species dominate at low coverage, while the tetrameric assemblies prevail at

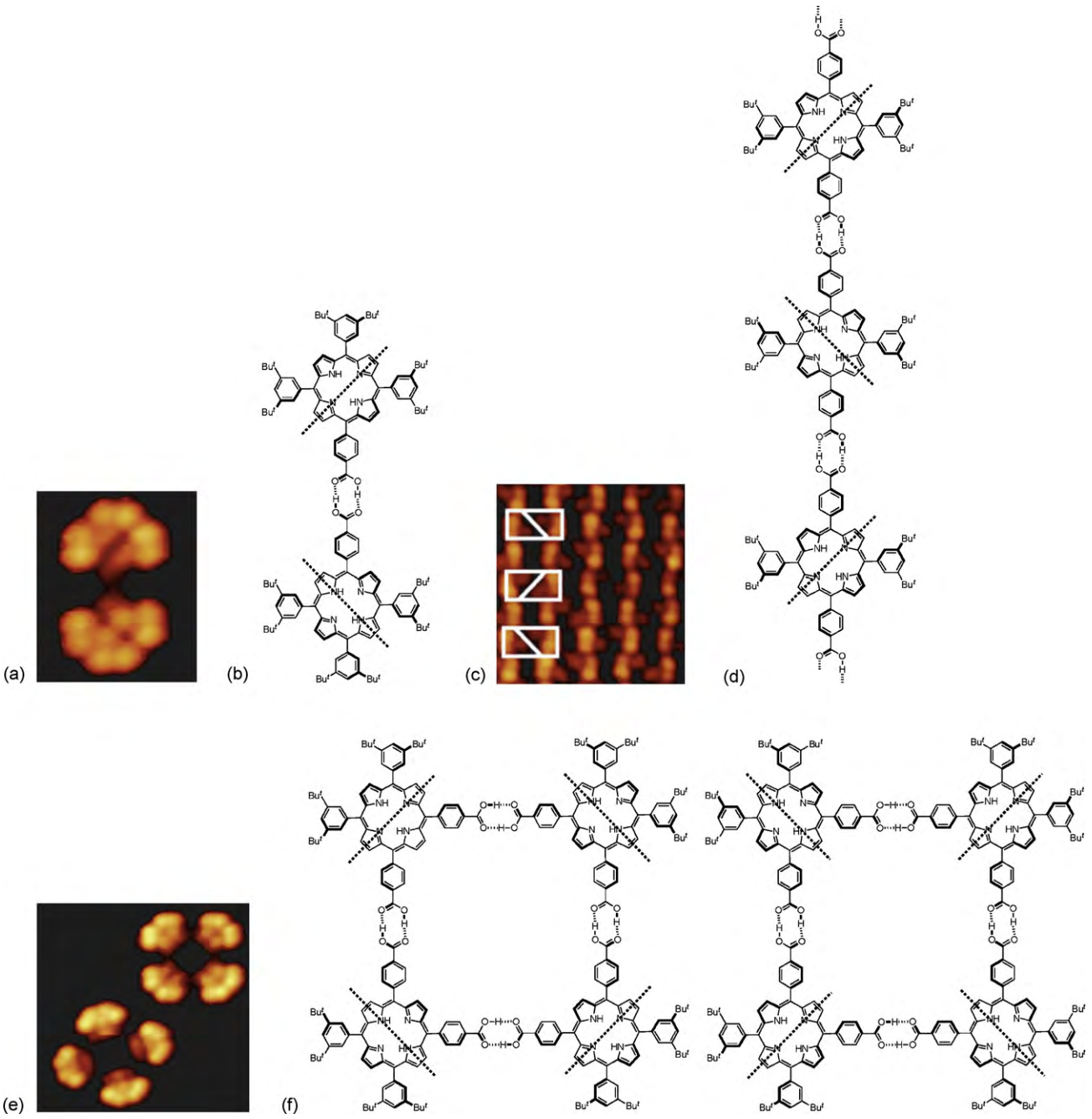

Fig. 23. Hydrogen-bonded assemblies and the conformations of porphyrins containing carboxyl groups on Au(1 1 1) [99,100]. (a and b) Dimer of H_2-$(HO_2CP)(DBP)_3P$. (c and d) Chain of *trans*-H_2-$(HO_2CP)_2(DBP)_2P$. (e and f) Tetrameric square from *cis*-H_2-$(HO_2CP)_2(DBP)_2P$. There are two conformational isomers with regard to distortion. Reproduced with permission from Ref. [99].

higher coverages. At high coverages, even pentameric and hexameric assemblies occur. The molecules of *trans*-$(PyCCP)_2(DBP)_2P$ form polymeric linear arrays as expected. Mixtures of the *trans* and *cis* molecules produce various parallelogram structures, the corners and the sides being provided by *cis*-$(PyCCP)_2(DBP)_2P$ and *trans*-$(PyCCP)_2(DBP)_2P$, respectively. Selective formation of one of these structures has not been achieved yet, as the assembly process is statistical in nature.

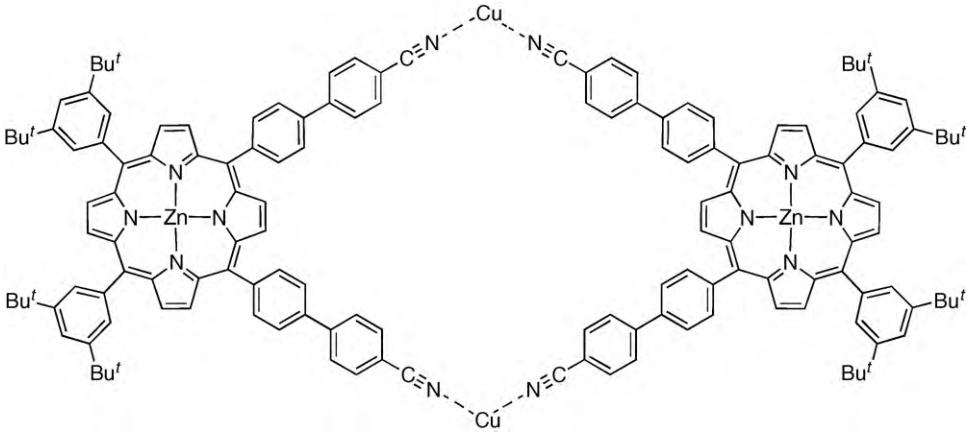

Fig. 24. Porphyrin dimer bridged by Cu atoms [98].

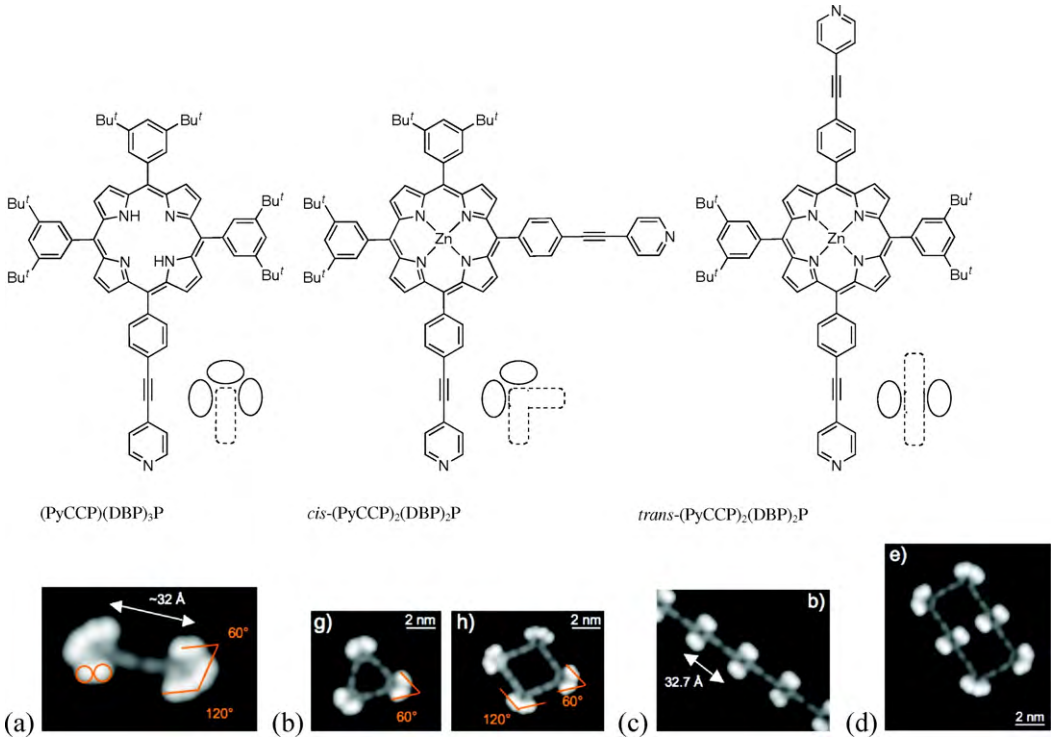

Fig. 25. Supramolecular architectures from porphyrins containing cyanophenyl groups on Cu(1 1 1). (a) (PyCCP)(DBP)$_3$P. (b) *cis*-(PyCCP)$_2$(DBP)$_2$P. (c) *trans*-(PyCCP)$_2$(DBP)$_2$P. (d) Mixture of *cis*- and *trans*-(PyCCP)$_2$(DBP)$_2$P. Reproduced with permission from Ref. [101].

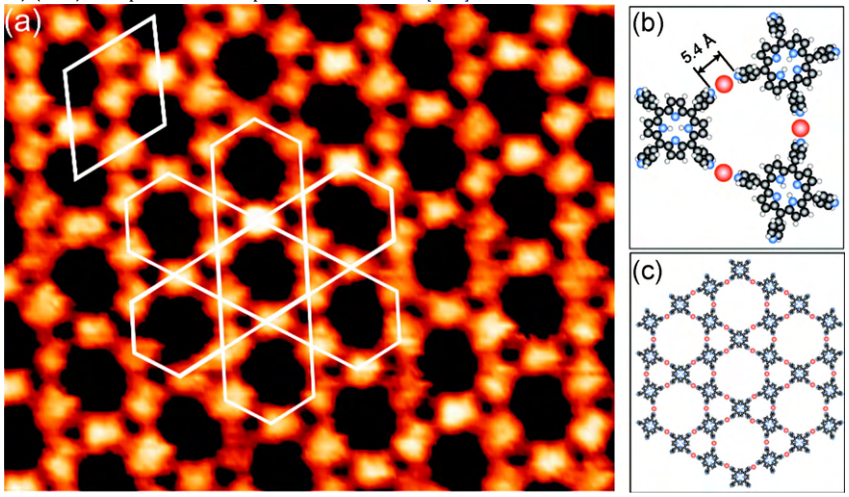

Fig. 26. Kagome lattice from H_2-TPyP on Au(1 1 1). STM image: 25 nm × 20 nm. Reproduced with permission from Ref. [102].

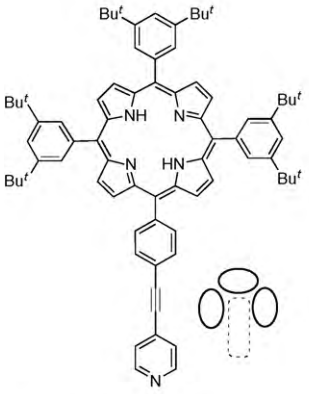

(PyCCP)(DBP)$_3$P

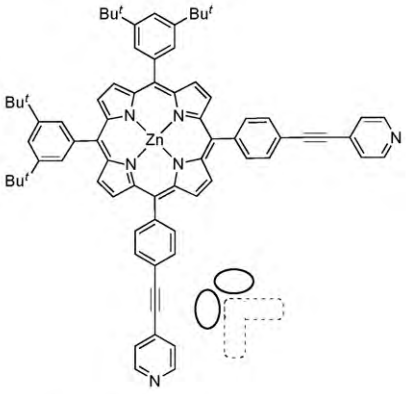

cis-(PyCCP)$_2$(DBP)$_2$P

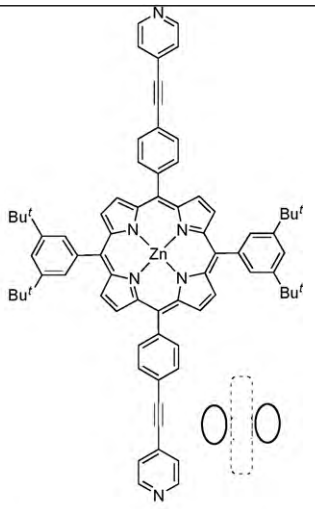

trans-(PyCCP)$_2$(DBP)$_2$P

Sublimation of H_2-TPyP on the Au(1 1 1) surface lead to a porous network with a kagome lattice motif, which is a geometric arrangement consisting of interconnected triangles and hexagons [102]. A model involving Au atom coordination has been proposed to account for the network formation as shown in Fig. 26. The STM observation indicated that the lifting of Au(1 1 1) reconstruction occurs under the network. It is speculated that the excess Au atoms accompanying the lifting of reconstruction are the source of the coordinated Au atoms.

4.3. Assemblies of elaborate porphyrin derivatives on metal surfaces

It is difficult to evaporate large molecules because their vapor pressures are so low that elevated temperatures are required to evaporate them, at which thermal decomposition may likely to occur. A pulse injection method has been developed to deposit molecules on surfaces under UHV conditions without exposing the sample to high temperatures [103,104].

Bithiophene modified tris(porphyrinato)cerium(III) triple-decker complexes, (B(BT)P)Ce(B(BT)P)Ce(B(BT)P), were deposited on the Au(1 1 1) surface with the pulse injection method [105]. The triple-decker molecules undergo face-on adsorption, forming linear network with some branches. The linear network extends along the herringbone structure characteristic of the reconstructed Au(1 1 1) surface.

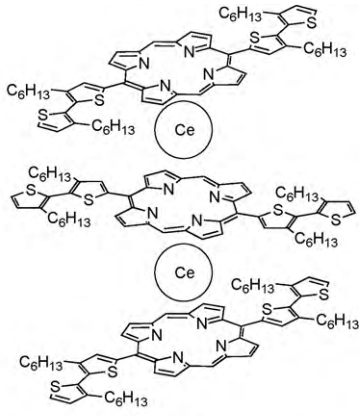

(B(BT)P)Ce(B(BT)P)Ce(B(BT)P)

A porphyrin 21mer, P_{21}-bandanna, shaped like a Bandanna having a Mandala pattern, was prepared through a 17-step synthesis with a total yield of 0.15% and was deposited on the Cu(1 1 1) surface using the pulse injection technique [106]. The STM revealed a collection of spots representing every porphyrin subunit in the square array spanning an area of 6.5 nm × 6.5 nm as shown in Fig. 27a A square cyclic porphyrin dodecamer, cyc-P_{12}, was also prepared and visualized by STM with a submolecular resolution, see Fig. 27b [107].

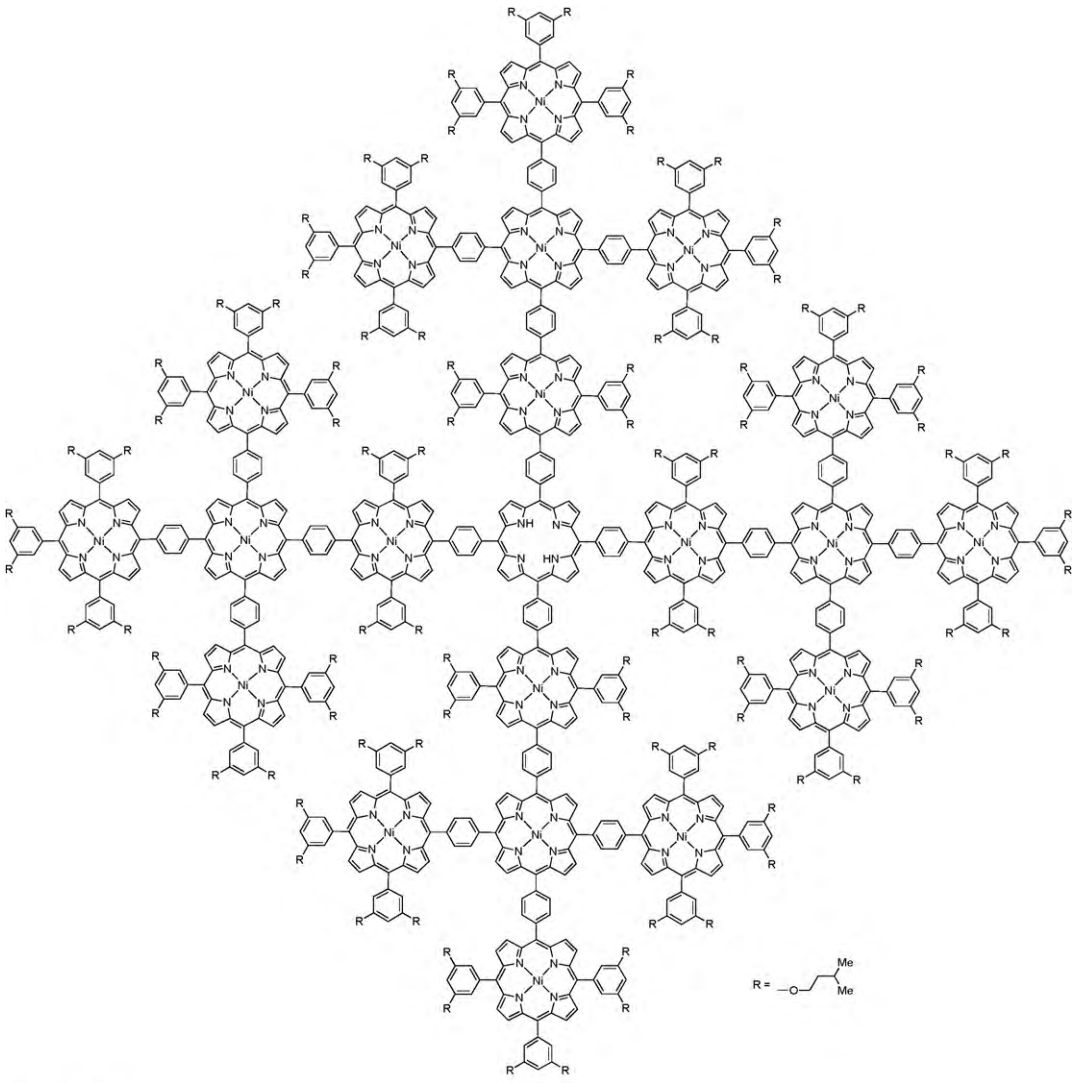

P21-bandanna

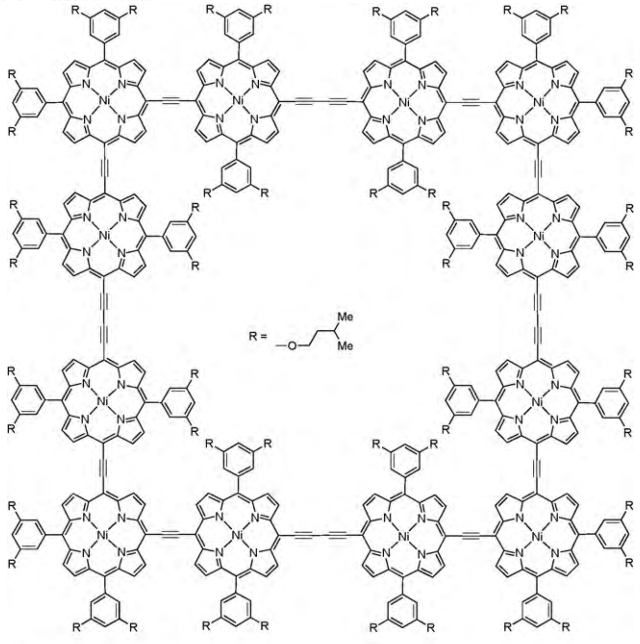

cyc-P_{12}

A dendrimer containing a porphyrin moiety at the center, P-dend, adsorbed on Au(1 1 1) was visualized with STM under ambient conditions [108]. On bare Au(1 1 1), the dendrimer is easily moved with the STM tip even at low scanning currents. Observed images at low temperatures indicate that the protrusion representing the dendrimers is rather flat and spread out. Mixtures of 1-hexadecanthiol and the dendrimer were used to overcome the problem of mobility. The dendrimers are embedded in the chemisorbed self-assembled monolayer (SAM) of 1-hexadecanthiol (Fig. 28). Thus the mobility of the dendrimer is suppressed and the dendrimer was successfully visualized with STM. The image gives a rounded protrusion that match the size of the dendrimer.

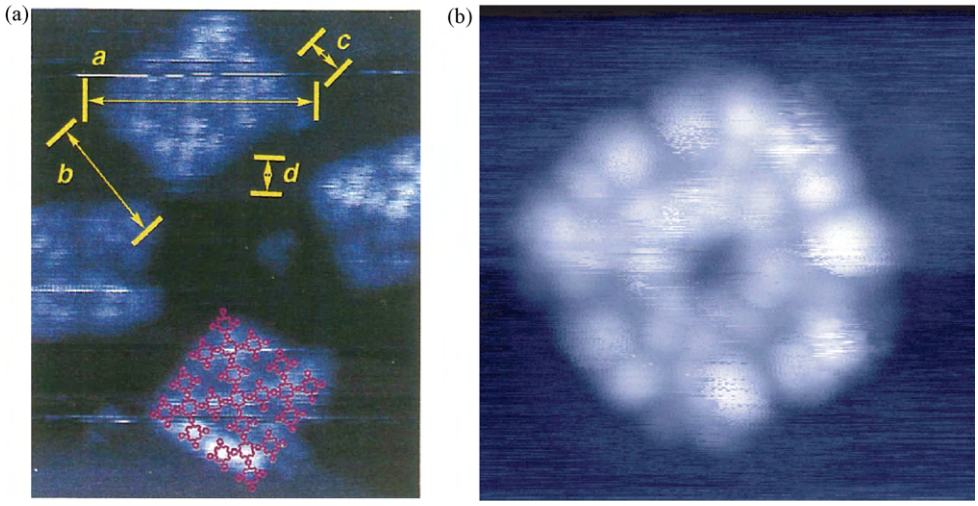

Fig. 27. Single molecular images of porphyrin multimers. (a) P_{21}-bandanna. The diagonal length, a = 9.5 nm. (b) cyc-P_{12}, 7 nm × 7 nm. Reproduced with permission from Refs. [106] (a) and [107] (b).

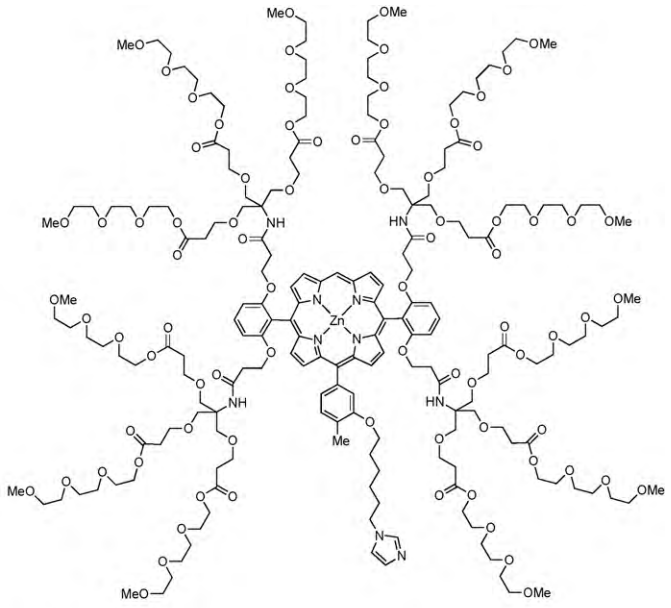

P-dend

4.4. In-situ reactions of porphyrins on metal surfaces

Sublimation methods have been applied to the preparation not only of physisorbed layers but also of chemisorbed layers, in which molecules are covalently attached to the substrate surface. An acetyl protected thiol derivative of porphyrin, H_2-T(ATMP)P, was vacuum deposited on the Ag(1 0 0) surface [109]. STM revealed the presence of large aggregates of porphyrin molecules on the surface at this stage. Upon annealing, the porphyrin aggregates disperse to form clusters of individual porphyrin molecules. Remarkably, the acetyl groups detached from the porphyrin and spread over the surface were also observed by STM. By the thermal annealing, deacetylation occurs and the S–Ag bond forms. Due to the covalent attachment of the molecules to the surface, the mobility of the molecules is low. Subsequent low-pressure oxygen introduction increases the mobility of the molecules, probably due to oxidation of S atoms, resulting in spread out porphyrin layers. Recently, this method was applied to prepare layers of catalytically active manganese porphyrins, Mn(III)Cl-T(ATMP)P [110].

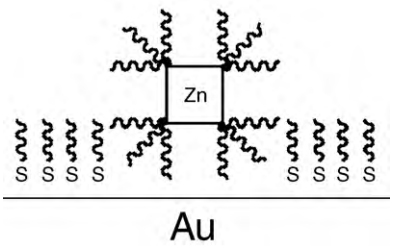

Fig. 28. Immobilization of P-dend on Au(1 1 1) supported by SAM [108].

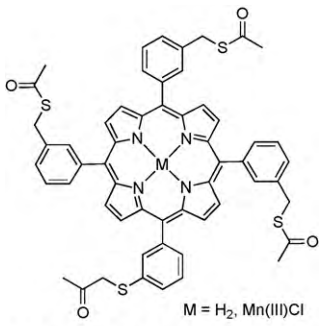

M-T(ATMP)P

Direct synthesis of metalloporphyrin complexes on surfaces has been demonstrated. Evaporation deposition of H_2-TPP on the Ag(1 1 1) substrate produces well-ordered arrays of the free-base porphyrin molecules. Subsequent evaporation deposition of cobalt metal results in the formation of Co-TPP on the surface [111,112]. The formal net reaction is two-electron oxidation of cobalt with concomitant reduction of the inner-ring protons of porphyrin: Co(0) + H_2-TPP → Co(II)-TPP + H_2. Porphyrin complexes with Zn [112] and Fe [113–115] were likewise prepared. The success of in-situ preparation of Fe porphyrin is particularly important because it is difficult to deposit clean Fe porphyrin via direct sublimation due to its high reactivity. For the Zn-porphyrin system, further evaporation of NH_3 molecules lead to the formation of the NH_3-coordinated Zn-porphyrin, demonstrating the feasibility of multistep in-situ synthesis on a surface [116].

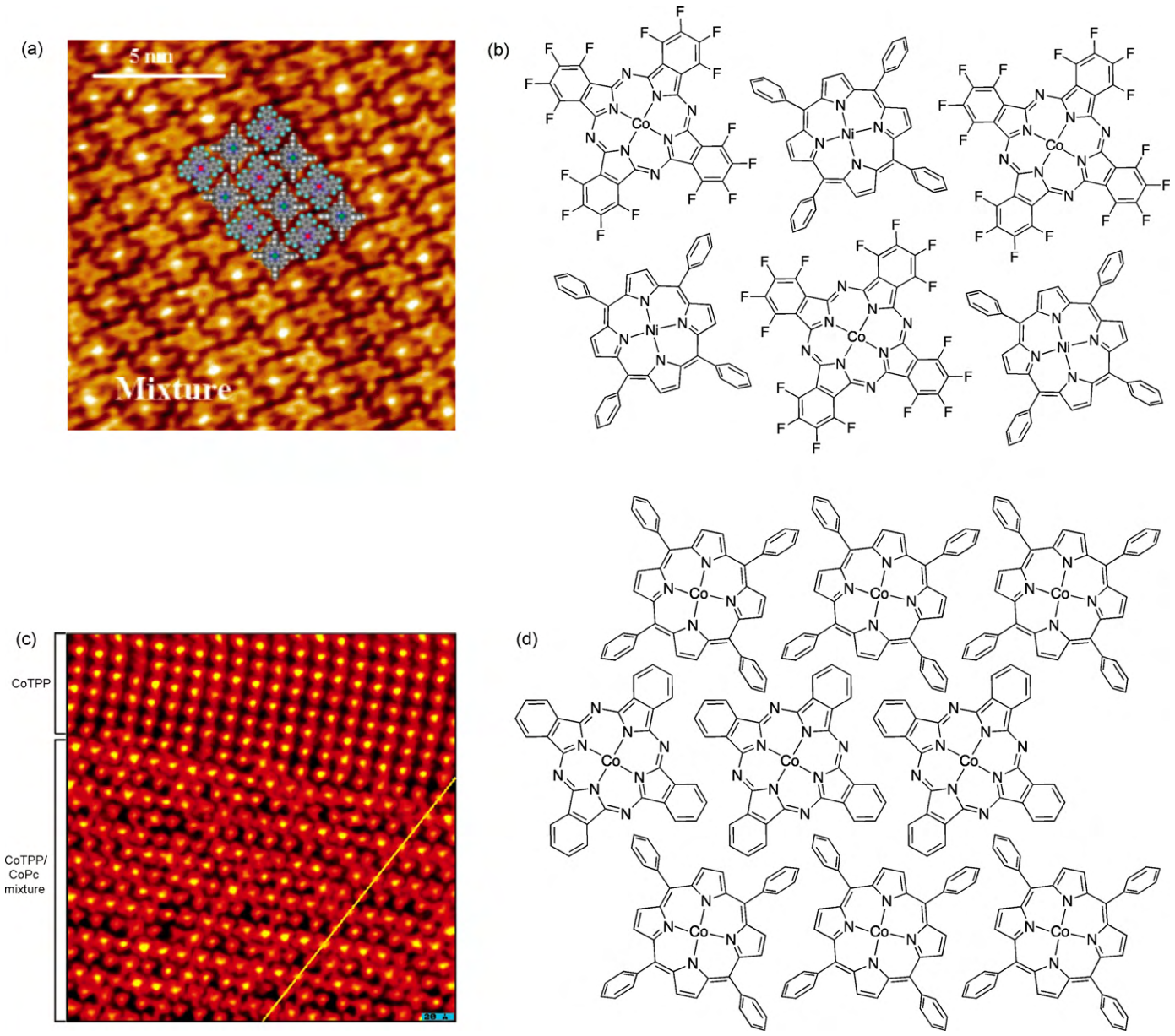

Fig. 29. Coassemblies of TPP and Pc derivatives. (a and b) Ni-TPP and Co-FPc [117,118]. (c and d) Co-TPP and Co-Pc [119]. Reproduced with permission from Refs. [117] (a) and [119] (c).

4.5. Multicomponent assemblies on metal surfaces

The fluorine-substituted aromatic–aromatic interactions were utilized to produce a well-ordered 1:1 mixed assembly on the Au(1 1 1) surface [117,118]. While Ni-TPP forms an ordered array on the Au(1 1 1) surface, a fluorinated phthalocyanine derivative, Co-FPc, does not. Upon codeposition of these two compounds, a well-ordered 1:1 chessboard-type assembly is formed as shown in Fig. 29a. One of the possible factors for the assembly formation is the attractive interactions between the fluorine and hydrogen atoms on the periphery of the molecules. These behaviors of Co-FPc contrast sharply with the protonated counterpart, Co-Pc. Co-Pc forms a well-ordered assembly by itself. Co-Pc also forms a densely packed well-defined structure with Ni-TPP, but it is compositionally disordered.

Deposition of Co-TPP and Co-Pc produces a 1:1 assembly as shown in Fig. 29c [119]. In this case, long rows of identical molecules

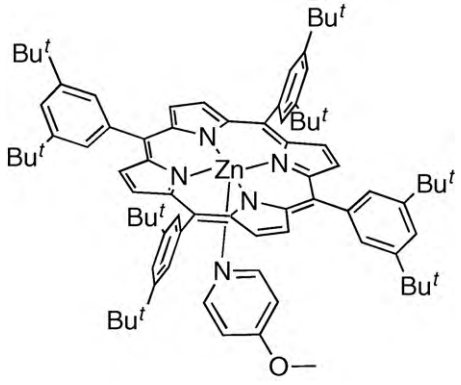

Fig. 30. Molecular pinwheel made of Zn-T(DBP)P attached on Ag(1 0 0) through axial coordination [120].

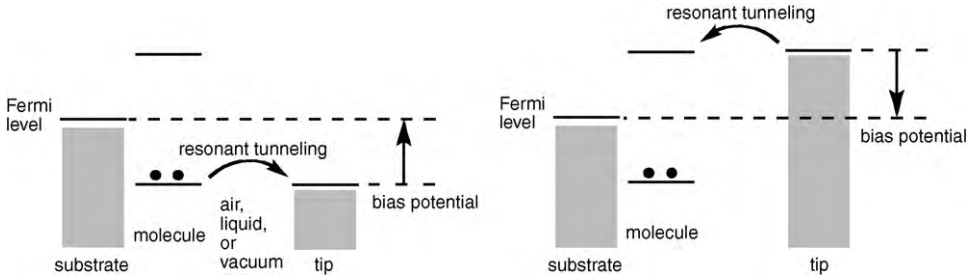

Fig. 31. Resonant tunneling at negative (left) and positive (right) sample bias voltages.

alternate. The packing is tighter in the assembly of Ni-TPP/Co-FPc than in that of Co-TPP/Co-Pc. The tighter binding may be driven by the H bonds involving fluorine.

Axial coordination may be exploited to construct molecular rotors making use of the rotatable nature of the bond formed between the metal and the axial ligand. Deposition of Zn-T(DBP)P on Ag(1 0 0) by evaporation in a UHV chamber gives four-lobed entities with a dip in the center as observed with STM [82]. Subsequent evaporation of DABCO to the porphyrin modified surface at 123 K makes the four-lobed features into higher, featureless protrusions, which are assigned as DABCO-ligated porphyrins. The assignment was supported by the observation that increasing temperature to 298 K makes the protrusions back into the four-lobed entities. It is reported that the sequence can be repeated many times on the same porphyrin covered surface. When 4-methoxypyridine was evaporated instead of DABCO, toroidal species appeared, which is higher than the ligand-free Zn-porphyrin but still has a depression at the center [120]. The newly appeared species is attributed to a Zn-porphyrin axially coordinated from underneath by 4-methoxypyridine, which is adsorbed to the Ag surface as shown in Fig. 30. The methoxy group is thought to be responsible for the surface binding, whereas the pyridine nitrogen is responsible for the axial coordination to the Zn-porphyrin. The toroidal image lacks the four-lobed feature, which suggests that the porphyrin molecules are rotating faster than the time scale of the STM measurement. As such, the system was termed as “a molecular pinwheel”.

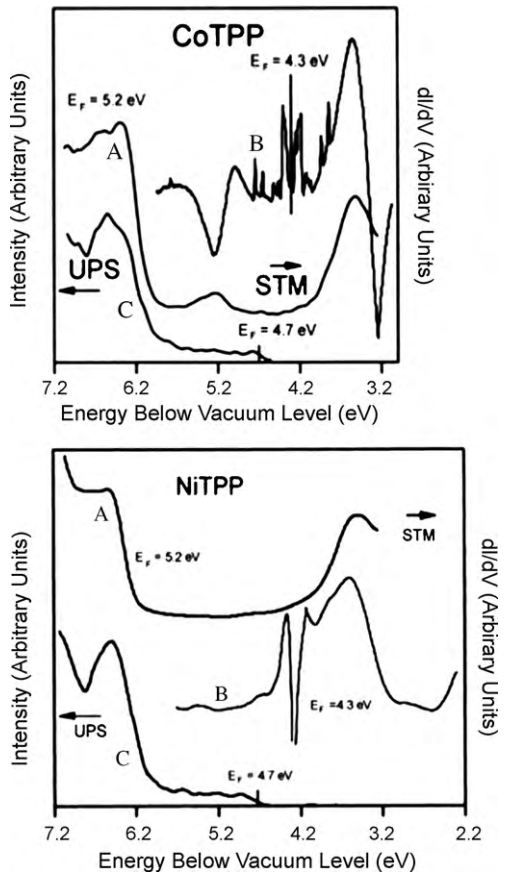

Fig. 32. STS for Co-TPP (top) and Ni-TPP (bottom) on the Au(1 1 1). Compare curve A's and note that a small peak at 5.2 eV, which corresponds to the bias voltage of −0.1 V, appears only for Co-TPP. Reproduced with permission from Ref. [127].

4.6. STM investigation on molecular electronic structures

The most widely used mode of operation in STM measurements is a constant current mode, in which the current value is kept constant at a specified value under a specified bias voltage by a feedback control on the *z*-position during scanning in the *xy* plane. As such, STM samples electronic as well as geometrical information localized below the tip at a molecular to atomic resolution.

In STS measurements, the current is measured as a function of the bias voltage with a tip being kept at a position after the feedback loop is cut off. The obtained *I*–*V* curve or d*I*/d*V*–*V* curve gives valuable insights into the electronic structure of the molecule under

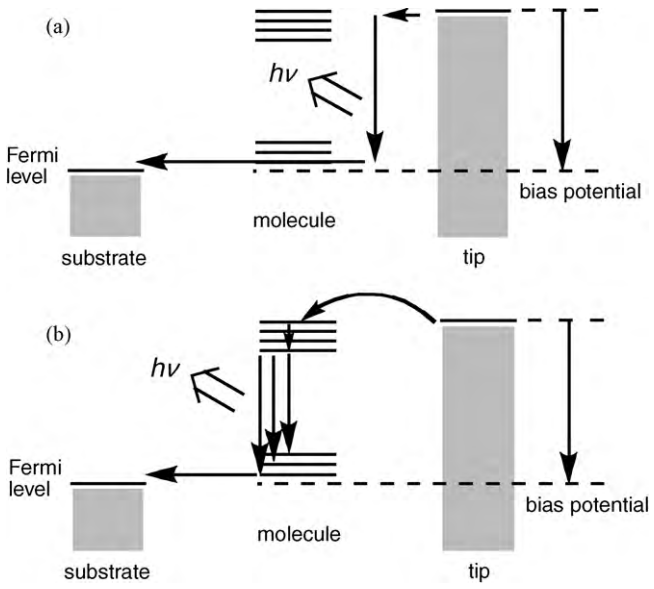

Fig. 33. Mechanisms of STM-induced light emission. (a) Inelastic tunneling channel. An electron from the tip inelastically tunnels through with simultaneous excitation of a plasmon. (b) Luminescence channel. An electron from the tip tunnels through elastically to excite the molecule. Vibrational relaxation within the same electronic level is followed by a radiative transition to the lowest electronic level. The vibrational structure may appear in the spectra due to the vibrational levels in the lowest electronic level. Note that horizontal lines for the molecule indicate not the orbital energies but the state energies. Also note that the luminescence is either from an anionic (one-electron reduced) state or from the neutral state of the molecule.

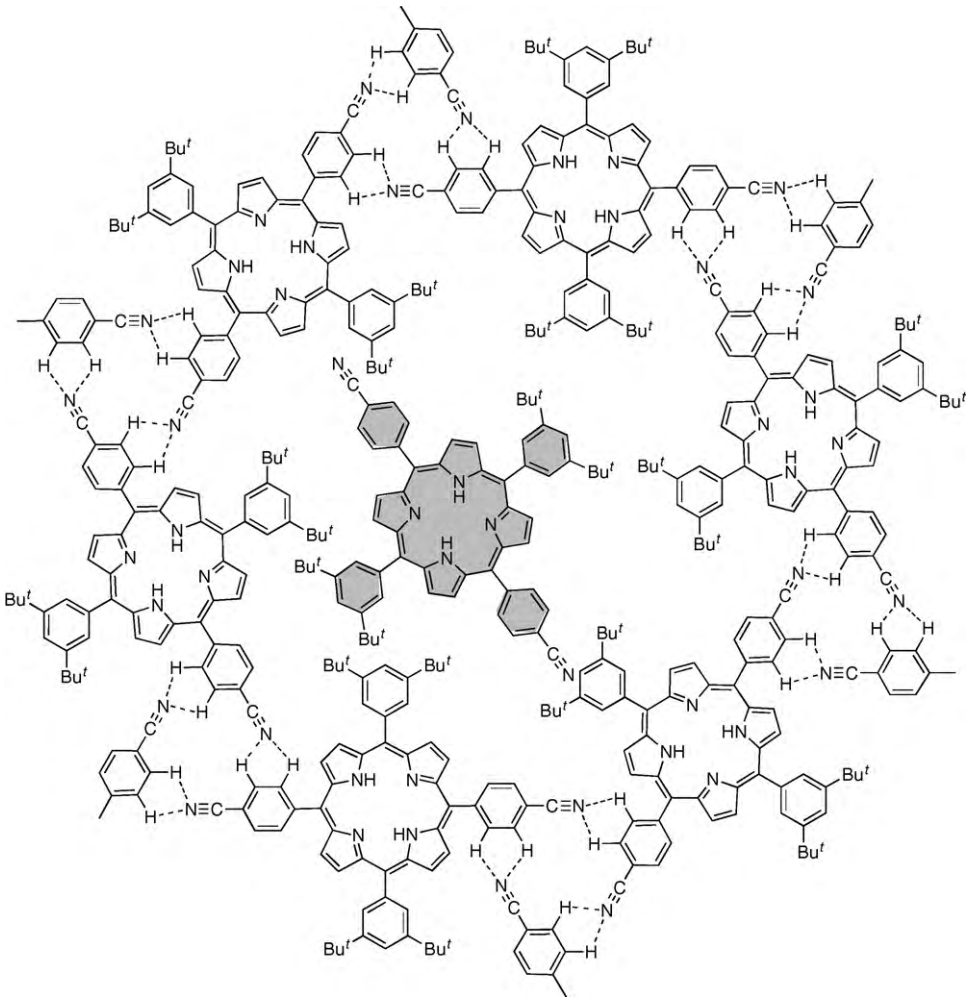

Fig. 34. Trapped Zn-$(NCP)_2(DBP)_2$P molecule change the orientation within the hexagonal pore [146].

the tip. In general, the tunnel current increases as the bias voltage is increased. When a molecule is present between the tip and the substrate surface, abrupt increase is observed at certain voltages as indicated by peaks in the dI/dV–V curve. The peak in the dI/dV–V curve indicates the occurrence of resonance tunneling between the molecule and the tip. The situation is illustrated in Fig. 31.

STM images for Co-TPP molecules show a protrusion at the metal site, while those for Ni-TPP does not [121]. Similar results were also observed for metal complexes of phthalocyanines [122–126]. STS was applied to Co-TPP [127], Ni-TPP [127], and Ni-OEP [128] adsorbed on the Au(1 1 1). The STS of the Co-porphyrin shows peaks at +1.7, −0.1, and −1.2 V bias voltages (Fig. 32). These peaks arise from orbital mediated tunneling involving unoccupied orbitals, the half-filled d(z^2) orbital on the cobalt atom, and occupied orbitals, respectively. The STS of the Ni-porphyrins shows peaks at +1.7 to +1.8 V and −1.2 to −1.3 V, corresponding respectively to unoccupied orbitals and occupied orbitals. The peak at the smaller bias observed for the Co-porphyrin is missing for the Ni-porphyrins, whose d(z^2) orbital is filled.

The orbital level at −0.1 V observed for the Co-porphyrin is responsible for the observed protrusion at the Co atom site, because the density of states near the Fermi level makes the largest contribution to the tunnel current [129]. The spatial orientation of the d(z^2) orbital, which extends along the surface normal, may also work favorably to the flow of tunnel current. In addition, for the case of Co-TPP and Co-T(DBP)P adsorbed on the Ag(1 1 1) surface, photoelectron spectroscopy studies showed that a significant electronic interaction results in a transfer of electron density from the surface to the Co ion [130].

4.7. STM-induced photon emission from porphyrins on metal surfaces

The detection of photons induced by tunneling electrons in STM has attracted much attention. STM-induced photon emission from adsorbed molecules are of particular interest as the event might be considered as the final step in the light emission of organic light-emitting diodes (OLEDs), as well as a single molecule version of OLED.

Photon emission from metal surfaces is attributed to the radiative decay of plasmons [131]. Two pathways are invoked for the excitation of plasmons in the STM configuration. One is inelastic tunneling, in which tunneling electrons give away a fraction of the energy to the plasmon (Fig. 33a). The other is hot electron thermalization (relaxation to the ground state), in which electrons tunnel through the barrier elastically and then give away the excess energy by thermalization. If a molecular excited state is involved in this process, the light emitted is identified as the luminescence from the molecule (Fig. 33b).

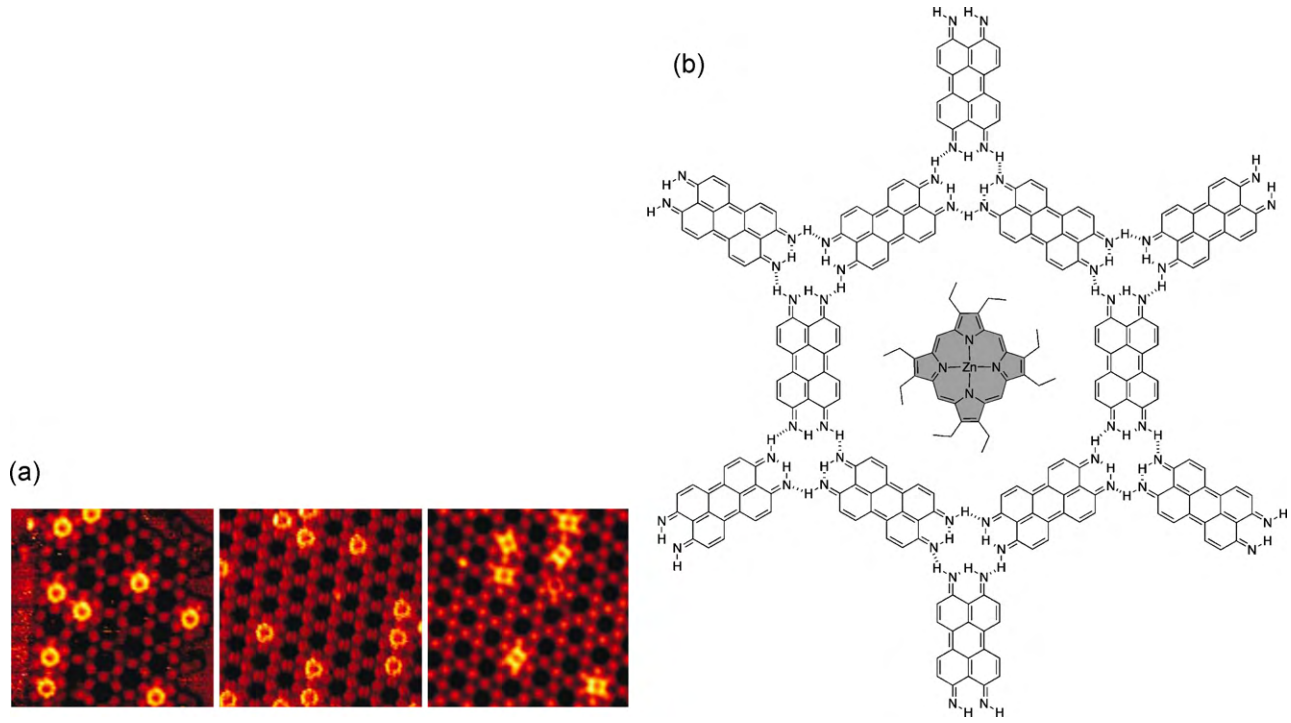

Fig. 35. Zn-OEP molecule trapped inside a pore of a hexagonal network on Cu(1 1 1). (a) STM images obtained at room temperature (left), 77 K (middle), and 5 K (right). 16 nm × 16 nm. Reproduced with permission from Ref. [147]. (b) Molecular structure.

Photon emission induced by tunneling electrons was studied for a monolayer of Cu-T(DBP)P adsorbed on the Cu(1 0 0) surface in UHV [131–134]. In earlier works, the involvement of molecular excited states was invoked to explain the observed enhancement of the light emission and its spectroscopic shift [132–134]. However, these data were later explained by modifications in the tip–substrate geometry in the presence of the molecule [131]. Only similar spectroscopic changes were observed even when intrinsically luminescent free-base porphyrin was used [135].

Fluorescence from an adsorbed molecule, if any, may be strongly quenched by the metal surface. An oxide layer was used to decouple the electronic states between the molecules and the metal surface and reduce the quenching by the metal surface. Specifically, an oxide layer was grown on NiAl(1 1 0), on which Zn(II) etioporphyrin I was thermally sublimed [136]. While the light-emission spectra were similar in shape to those from the bare NiAl(1 1 0) surface for the molecules deposited directly on the NiAl(1 1 0) surface, distinct light-emission features of molecular origin were observed for the molecules deposited on the oxide surface. The molecular nature of the detected luminescence was proved by the appearance of vibrational structure that match that of photoluminescence of the molecule, or the Zn(II) etioporphyrin I monoanion in this particular case.

Another method employed to decouple the metal surface and the molecules is to use multilayers, where the topmost layers are decoupled with the metal surface by the underlying molecules. For example, layers of Pt-T(DBP)P molecules were grown on the surface of Cu(1 0 0) before deposition of a layer of H_2-T(DBP)P molecules [137]. From this multilayer, STM-induced luminescence was observed. The spectroscopic shape was similar to that of photoluminescence of H_2-T(DBP)P (the neutral molecule in this case), indicating that the observed STM-induced luminescence emanates from the topmost layer. Multilayer strategy to observe STM-induced luminescence was confirmed to work for several other systems including a multilayer of H_2-T(DBP)P on Au(1 0 0) [138,139], a layer of H_2-T(DBP)P molecules on top of a multilayer of H_2-T(FP)P molecules on Cu(1 0 0) [140], and a multilayer of Zn-T(DBP)P molecules on Cu(1 0 0) [139].

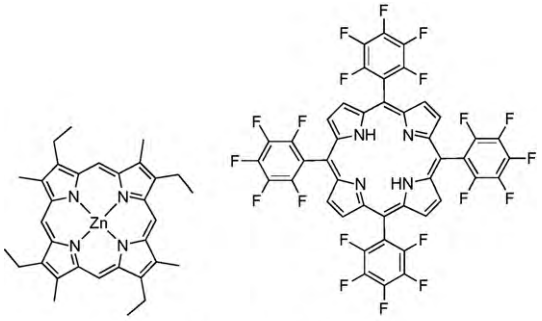

4.8. Motions of individual porphyrin molecules

Closely related to molecular electronics are molecular machines [141–145], which have been attracting much attention in the pursuit for ever smaller machines. Molecular rotors would be one of the elementary components of molecular machines.

cis-Zn-$(NCP)_2(DBP)_2$P molecules assemble into a hexagonal porous network on the Cu(1 1 1) surface [146], through CN...H hydrogen bonds, which are also observed on Au(1 1 1) [96]. A molecule is found in some of the pores, which is trapped in the pore but does not participate in the hydrogen-bonded network as shown in Fig. 34. The molecule has a two-fold symmetry and the pore has a six-fold symmetry. Therefore, there are three equivalent orientations for the trapped molecule. The molecule can change its orientation by rotational motion within the pore. Temperature dependent rate of orientation change was examined to give an activation energy of 0.24 eV with a frequency factor of $5 \times 10^7\ s^{-1}$. The orientation change can also be induced with the STM tip. A pulse of $V = -0.7$ V and $I = 150$ pA for 1 s causes an orientation change at 77 K,

at which temperature no thermally induced orientation change takes place.

Thermal dehydrogenation of 4,9-diaminoperylene-quinone-3,10-diimine on a Cu(1 1 1) surface leads to the formation of a highly stable hexagonal molecular network. The hexagonal holes can trap guest molecules of appropriate shape and size [147]. Zn-OEP is trapped within the hole as shown in Fig. 35. Due to its four-fold symmetry, there are three equivalent orientations of the porphyrin molecule with respect to the hexagonal network. At room temperature, the porphyrin molecule is observed as a ring due to its fast rotational motion. At 77 K, the rings become noisy, indicating comparable rate of rotational motion with the STM time scale. Finally, at 5 K, the dynamic motion is frozen, revealing a rectangular shape of the Zn-OEP molecules. The analysis of the temperature dependence yielded an activation energy of 0.17 eV and a frequency factor of $10^{10.5}$ s^{-1} for the orientation change.

5. Conclusions and prospect

STM studies on porphyrins have been described. The submolecular resolution of STM has yielded information on individual molecules that cannot be obtained with other means. STM measured tunneling current that is determined by the local electronic states between the tip and the substrate. Valuable information on the electronic structure of a molecule or even that of a part of the molecule can be gleaned from the analysis of the topographical images and *I–V* characteristics. Capability of manipulating molecules adds additional values to STM.

Porphyrins are one of the most promising components for future electronic devices and materials including molecular electronics, considering their rich electronic and photonic properties. The power of self-assembly and the amiability to surfaces are additional benefits for constructing device structures. Conformational flexibility and manipulability further extend the possibility of tuning and controlling their properties. These aspects have been revealed by STM studies on individual porphyrin molecules.

As described in the introduction, there is a long way to go until we can make molecular electronics devices. Key issues to be addressed are those indicated by words with plain letters (not bold) in Fig. 1: Electronic communication among molecules in ordered surface assemblies should be revealed; modulation of the electronic communication by designed surface assemblies should be realized; and, finally, probably as the most difficult step, nonperiodic surface assemblies should be prepared that work as a molecular electronic circuit.

Acknowledgement

Financial support from the Nihon University "*N*." Research Project, Nanotechnology Excellence and the MEXT, Japan through the programs of Grant-in-Aid for Scientific Research is greatly appreciated.

References

[1] J.M. Tour, Acc. Chem. Res. 33 (2000) 791.
[2] Y. Wada, M. Tsukada, M. Fujihira, K. Matsushige, T. Ogawa, M. Haga, S. Tanaka, Jpn. J. Appl. Phys. 39 (2000) 3835.
[3] C. Joachim, J.K. Gimzewski, A. Aviram, Nature 408 (2000) 541.
[4] R.L. Carroll, C.B. Gorman, Angew. Chem. Int. Ed. 41 (2002) 4378.
[5] R.M. Metzger, J. Mater. Chem. 18 (2008) 4364.
[6] J.-M. Lehn, Supramolecular Chemistry: Concept and Perspectives, VCH, Weinheim, 1995.
[7] K. Ariga, J.P. Hill, M.V. Lee, A. Vinu, R. Charvet, S. Acharya, Sci. Technol. Adv. Mater. 9 (2008) 014109.
[8] J. Frommer, Angew. Chem. Int. Ed. 31 (1992) 1298.
[9] S. Yoshimoto, Bull. Chem. Soc. Jpn. 79 (2006) 1167.
[10] M. Ruben, J.-M. Lehn, P. Müller, Chem. Soc. Rev. 35 (2006) 1056.
[11] N. Miyashita, D.G. Kurth, J. Mater. Chem. 18 (2008) 2636.
[12] D. Bonifazi, S. Mohnani, A. Llanes-Pallas, Chem. Eur. J. 15 (2009) 7004.
[13] K. Petukhov, M.S. Alam, H. Rupp, S. Stroemsdoerfer, P. Mueller, A. Scheurer, R.W. Saalfrank, J. Kortus, A. Postnikov, M. Ruben, L.K. Thompson, J.-M. Lehn, Coord. Chem. Rev. 253 (2009) 2387.
[14] J.V. Barth, Surface Sci. 603 (2009) 1533.
[15] J.S. Foster, J.E. Frommer, Nature 333 (1988) 542.
[16] D.P.E. Smith, J.K.H. Hörber, G. Binnig, H. Nejoh, Nature 344 (1990) 641.
[17] D.P.E. Smith, H. Hörber, C. Gerber, G. Binnig, Science 245 (1989) 43.
[18] L.C. Giancarlo, G.W. Flynn, Acc. Chem. Res. 33 (2000) 409.
[19] S. De Feyter, J. Hofkens, M. Van der Auweraer, R.J.M. Nolte, K. Müllen, F.C. Schryver, Chem. Commun. (2001) 585.
[20] D.M. Cyr, B. Venkataraman, G.W. Flynn, Chem. Mater. 8 (1996) 1600.
[21] S. De Feyter, F.C. De Schryver, Chem. Soc. Rev. 32 (2003) 139.
[22] S. De Feyter, F.C. De Schryver, J. Phys. Chem. B 109 (2005) 4290.
[23] S. Yin, C. Wang, X. Qiu, B. Xu, C. Bai, Surf. Interface Anal. 32 (2001) 248.
[24] C. Liu, H. Chang, A.J. Bard, Langmuir 7 (1991) 1138.
[25] H. Chang, A.J. Bard, Langmuir 7 (1991) 1143.
[26] C.R. Clemmer, T.P. Beebe Jr., Science 251 (1991) 640.
[27] W.-T. Pong, C. Durkan, J. Phys. D: Appl. Phys. 38 (2005) R329.
[28] Y. Wang, Y. Ye, K. Wu, Surface Sci. 600 (2006) 729.
[29] N.J. Tao, G. Cardenas, F. Cunha, Z. Shi, Langmuir 11 (1995) 4445.
[30] X. Qiu, C. Wang, Q. Zeng, B. Xu, S. Yin, H. Wang, S. Xu, C. Bai, J. Am. Chem. Soc. 122 (2000) 5550.
[31] H. Wang, C. Wang, Q. Zeng, S. Xu, S. Yin, B. Xu, C. Bai, Surf. Interface Anal. 32 (2001) 266.
[32] S.B. Lei, J. Wang, Y.H. Dong, C. Wang, L.J. Wan, C.L. Bai, Surf. Interface Anal. 34 (2002) 767.
[33] J. Otsuki, K. Namiki, Y. Arai, M. Amano, H. Sawai, A. Tsukamoto, T. Hagiwara, Chem. Lett. 38 (2009) 570.
[34] M. Linares, P. Iavicoli, K. Psychogyiopoulou, D. Beljonne, S.D. Feyter, D.B. Amabilino, R. Lazzaroni, Langmuir 24 (2008) 9566.
[35] B. Hulsken, R.V. Hameren, P. Thordarson, J.W. Gerritsen, R.J.M. Nolte, A.E. Rowan, M.J. Crossley, J.A.A.W. Elemans, S. Speller, Jpn. J. Appl. Phys. 45 (2006) 1953.
[36] N. Katsonis, J. Vicario, T. Kudernac, J. Visser, M.M. Pollard, B.L. Feringa, J. Am. Chem. Soc. 128 (2006) 15537.
[37] A. Ogunrinde, K.W. Hipps, L. Scudiero, Langmuir 22 (2006) 5697.
[38] L. Scudiero, K.W. Hipps, J. Phys. Chem. C 111 (2007) 17516.
[39] P. Iavicoli, S.-S. Maite, D.B. Amabilino, New J. Chem. 33 (2009) 358.
[40] T. Ikeda, M. Asakawa, K. Miyake, M. Goto, T. Shimizu, Langmuir 24 (2008) 12877.
[41] Y. Zhou, B. Wang, M. Zhu, J.G. Hou, Chem. Phys. Lett. 403 (2005) 140.
[42] Q.-M. Xu, L.-J. Wan, S.-X. Yin, C. Wan, C.-L. Bai, T. Ishii, K. Uehara, Z.-Y. Wang, T. Nozawa, J. Phys. Chem. B 106 (2002) 3037.
[43] Y. Diskin-Posner, I. Goldberg, Chem. Commun. (1999) 1961.
[44] S.B. Lei, C. Wang, S.X. Yin, H.N. Wang, F. Xi, H.W. Liu, B. Xu, L.J. Wan, C.L. Bai, J. Phys. Chem. B 105 (2001) 10838.
[45] J. Otsuki, E. Nagamine, T. Kondo, K. Iwasaki, M. Asakawa, K. Miyake, J. Am. Chem. Soc. 127 (2005) 10400.
[46] C.M. Drain, F. Nifiatis, A. Vasenko, J.D. Batteas, Angew. Chem. Int. Ed. 37 (1998) 2344.
[47] T.N. Milic, N. Chi, D.G. Yablon, G.W. Flynn, J.D. Batteas, C.M. Drain, Angew. Chem. Int. Ed. 41 (2002) 2117.
[48] C.M. Drain, J.D. Batteas, G.W. Flynn, T. Milic, N. Chi, D.G. Yablon, H. Sommers, Proc. Natl. Acad. Sci. U.S.A. 99 (2002) 6498.
[49] M. Koepf, J.A. Wytko, J.P. Bucher, J. Weiss, J. Am. Chem. Soc. 130 (2008) 9994.
[50] J. Otsuki, S. Kawaguchi, T. Yamakawa, M. Asakawa, K. Miyake, Langmuir 22 (2006) 5708.
[51] T. Takami, T. Ye, D.P. Arnold, K. Sugiura, R. Wang, J. Jiang, P.S. Weiss, J. Phys. Chem. C 111 (2007) 2077.
[52] J.A.A.W. Elemans, M.C. Lensen, J.W. Gerritsen, H. van Kempen, S. Speller, R.J.M. Nolte, A.E. Rowan, Adv. Mater. 15 (2003) 2070.
[53] M.C. Lensen, S.J.T.v. Dingenen, J.A.A.W. Elemans, H.P. Dijkstra, G.P.M.v. Klink, G.v. Koten, J.W. Gerritsen, S. Speller, R.J.M. Nolte, A.E. Rowan, Chem. Commun. (2004) 762.
[54] M.C. Lensen, J.A.A.W. Elemans, S.J.T.v. Dingenen, J.W. Gerritsen, S. Speller, A.E. Rowan, R.J.M. Nolte, Chem. Eur. J. 13 (2007) 7948.
[55] P.C.M.v. Gerven, J.A.A.W. Elemans, J.W. Gerritsen, S. Speller, R.J.M. Nolte, A.E. Rowan, Chem. Commun. (2005) 3535.
[56] J. Otsuki, Trends Phys. Chem. 8 (2001) 61.
[57] T. Ikeda, M. Asakawa, M. Goto, K. Miyake, T. Ishida, T. Shimizu, Langmuir 20 (2004) 5454.
[58] J. Otsuki, E. Seki, T. Taguchi, M. Asakawa, K. Miyake, Chem. Lett. 36 (2007) 740.
[59] J. Visser, N. Katsonis, J. Vicario, B.L. Feringa, Langmuir 25 (2009) 5980.
[60] T. Ohshiro, T. Ito, P. Bühlmann, Y. Umezawa, Anal. Chem. 73 (2001) 878.
[61] T. Nishino, T. Ito, Y. Umezawa, Proc. Natl. Acad. Sci. U.S.A. 102 (2005) 5659.
[62] M. Kunitake, U. Akiba, N. Batina, K. Itaya, Langmuir 13 (1997) 1607.
[63] M. Kunitake, N. Batina, K. Itaya, Langmuir 11 (1995) 2337.
[64] K. Ogaki, N. Batina, M. Kunitake, K. Itaya, J. Phys. Chem. 100 (1996) 7185.
[65] K. Sashikata, T. Sugata, M. Sugimasa, K. Itaya, Langmuir 14 (1998) 2896.
[66] L.-J. Wan, S. Shundo, J. Inukai, K. Itaya, Langmuir 16 (2000) 2164.
[67] Y. He, T. Ye, E. Borguet, J. Am. Chem. Soc. 124 (2002) 11964.
[68] S. Yoshimoto, A. Tada, K. Suto, R. Narita, K. Itaya, Langmuir 19 (2003) 672.

[69] S. Yoshimoto, J. Inukai, A. Tada, T. Abe, T. Morimoto, A. Osuka, H. Furuta, K. Itaya, J. Phys. Chem. B 108 (2004) 1948.
[70] S. Yoshimoto, A. Tada, K. Suto, S.-L. Yau, K. Itaya, Langmuir 20 (2004) 3159.
[71] S. Yoshimoto, K. Sato, S. Sugawara, Y. Chen, O. Ito, T. Sawaguchi, O. Niwa, K. Itaya, Langmuir 23 (2007) 809.
[72] S. Yoshimoto, N. Yokoo, T. Fukuda, N. Kobayashi, K. Itaya, Chem. Commun. (2006) 500.
[73] S. Yoshimoto, T. Sawaguchi, W. Su, J. Jiang, N. Kobayashi, Angew. Chem. Int. Ed. 46 (2007) 1071.
[74] K. Suto, S. Yoshimoto, K. Itaya, J. Am. Chem. Soc. 125 (2003) 14976.
[75] S. Yoshimoto, Y. Honda, O. Ito, K. Itaya, J. Am. Chem. Soc. 130 (2008) 1085.
[76] S. Yoshimoto, N. Higa, K. Itaya, J. Am. Chem. Soc. 126 (2004) 8540.
[77] S. Yoshimoto, E. Tsutsumi, Y. Honda, O. Ito, K. Itaya, Chem. Lett. 33 (2004) 914.
[78] S. Yoshimoto, A. Saito, E. Tsutsumi, F. D'Souza, O. Ito, K. Itaya, Langmuir 20 (2004) 11046.
[79] N.J. Tao, Phys. Rev. Lett. 76 (1996) 4066.
[80] Y. He, E. Borguet, Angew. Chem. Int. Ed. 46 (2007) 6098.
[81] F. Buchner, K. Comanici, J. Norbert, H.-P. Steinrueck, H. Marbach, J. Phys. Chem. C 111 (2007) 13531.
[82] F.J. Williams, O.P.H. Vaughan, K.J. Knox, N. Bampos, R.M. Lambert, Chem. Commun. (2004) 1688.
[83] H. Yanagi, H. Mukai, K. Ikuta, T. Shibutani, T. Kamikado, S. Yokoyama, S. Mashiko, Nano Lett. 2 (2002) 601.
[84] F. Moresco, G. Meyer, K.-H. Rieder, H. Tang, A. Gourdon, C. Joachim, Phys. Rev. Lett. 87 (2001) 088302.
[85] T.A. Jung, R.R. Schlittler, J.K. Gimzewski, Nature 386 (1997) 696.
[86] L. Grill, I. Stass, K.-H. Rieder, F. Moresco, Surface Sci. 600 (2006) L143.
[87] F. Moresco, G. Meyer, K.-H. Rieder, H. Tang, A. Gourdon, C. Joachim, Phys. Rev. Lett. 86 (2001) 672.
[88] T. Terui, S. Yokoyama, H. Suzuki, S. Mashiko, M. Sakurai, T. Moriwaki, Thin Solid Films 499 (2006) 157.
[89] T. Yokoyama, S. Yokoyama, T. Kamikado, S. Mashiko, J. Chem. Phys. 115 (2001) 3814.
[90] C. Loppacher, M. Guggisberg, O. Pfeiffer, E. Meyer, M. Bammerlin, R. Lüthi, R. Schlittler, J.K. Gimzewski, H. Tang, C. Joachim, Phys. Rev. Lett. 90 (2003) 066107.
[91] W. Auwärter, A. Weber-Bargioni, A. Riemann, A. Schiffrin, O. Gröning, R. Fasel, J.V. Barth, J. Chem. Phys. 124 (2006) 194708.
[92] J.P. Hill, Y. Wakayama, K. Ariga, Phys. Chem. Chem. Phys. 8 (2006) 5034.
[93] Y. Wakayama, J.P. Hill, K. Ariga, Surface Sci. 601 (2007) 3984.
[94] J.P. Hill, Y. Wakayama, W. Schmitt, T. Tsuruoka, T. Nakanishi, M.L. Zandler, A.L. McCarty, F. D'Souza, L.R. Milgrom, K. Ariga, Chem. Commun. (2006) 2320.
[95] J.P. Hill, Y. Wakayama, M. Akada, K. Ariga, J. Phys. Chem. C 111 (2007) 16174.
[96] T. Yokoyama, S. Yokoyama, T. Kamikado, Y. Okuno, S. Mashiko, Nature 413 (2001) 619.
[97] N. Wintjes, J. Hornung, J. Lobo-Checa, T. Voigt, T. Samuely, C. Thilgen, M. Stöhr, F. Diederich, T.A. Jung, Chem. Eur. J. 14 (2008) 5794.
[98] L.-A. Fendt, M. Stöhr, N. Wintjes, M. Enache, T.A. Jung, F. Diederich, Chem. Eur. J. 15 (2009) 11139.
[99] T. Yokoyama, T. Kamikado, S. Yokoyama, S. Mashiko, J. Chem. Phys. 121 (2004) 11993.
[100] F. Nishiyama, T. Yokoyama, T. Kamikado, S. Yokoyama, S. Mashiko, Appl. Phys. Lett. 88 (2006) 253113.
[101] D. Heim, K. Seufert, W. Auwärter, C. Aurisicchio, C. Fabbro, D. Bonifazi, J.V. Barth, Nano Lett. 10 (2010) 122.
[102] Z. Shi, N. Lin, J. Am. Chem. Soc. 131 (2009) 5376.
[103] H. Tanaka, T. Kawai, J. Vac. Sci. Technol. B 15 (1997) 602.
[104] H. Tanaka, C. Hamai, T. Kanno, T. Kawai, Surface Sci. 432 (1999) L611.
[105] H. Tanaka, T. Ikeda, K. Yamashita, M. Takeuchi, S. Shinkai, T. Kawai, Langmuir 26 (2010) 201.
[106] K.-i. Sugiura, H. Tanaka, T. Matsumoto, T. Kawai, Y. Sakata, Chem. Lett. (1999) 1193.
[107] A. Kato, K.-i. Sugiura, H. Miyasaka, H. Tanaka, T. Kawai, M. Sugimoto, M. Yamashita, Chem. Lett. 33 (2004) 578.
[108] L. Merz, J. Hitz, U. Hubler, P. Weyermann, F. Diederich, P. Murer, D. Seebach, I. Widmer, M. Stöhr, H.-J. Guntherodt, B.A. Hermann, Single Mol. 5–6 (2002) 295.
[109] O.P.H. Vaughan, M. Turner, F.J. Williams, A. Hille, J.K.M. Sanders, R.M. Lambert, J. Am. Chem. Soc. 128 (2006) 9578.
[110] M. Turner, O.P.H. Vaughan, G. Kyriakou, D.J. Watson, L.J. Scherer, G.J.E. Davidson, J.K.M. Sanders, R.M. Lambert, J. Am. Chem. Soc. 131 (2009) 1910.
[111] J.M. Gottfried, K. Flechtner, A. Kretschmann, T. Lukasczyk, H.-P. Steinrueck, J. Am. Chem. Soc. 128 (2006) 5644.
[112] T.E. Shubina, H. Marbach, K. Flechtner, A. Kretschmann, N. Jux, F. Buchner, H.-P. Steinrück, T. Clark, J.M. Gottfried, J. Am. Chem. Soc. 129 (2007) 9476.
[113] F. Buchner, K. Flechtner, Y. Bai, E. Zillner, I. Kellner, H.-P. Steinrück, H. Marbach, J.M. Gottfried, J. Phys. Chem. C 112 (2008) 15458.
[114] F. Buchner, V. Schwald, K. Comanici, H.-P. Steinrueck, H. Marbach, ChemPhysChem 8 (2007) 241.
[115] W. Auwärter, A. Weber-Bargioni, S. Brink, A. Riemann, A. Schiffrin, M. Ruben, J.V. Barth, ChemPhysChem 8 (2007) 250.
[116] K. Flechtner, A. Kretschmann, L.R. Bradshaw, M.-M. Walz, H.-P. Steinrück, J.M. Gottfried, J. Phys. Chem. C 111 (2007) 5821.
[117] K.W. Hipps, L. Scudiero, D.E. Barlow, M.P. Cooke Jr., J. Am. Chem. Soc. 124 (2002) 2126.
[118] L. Scudiero, K.W. Hipps, D.E. Barlow, J. Phys. Chem. B 107 (2003) 2903.
[119] D.E. Barlow, L. Scudiero, K.W. Hipps, Langmuir 20 (2004) 4413.
[120] O.P.H. Vaughan, F.J. Williams, N. Bampos, R.M. Lambert, Angew. Chem. Int. Ed. 45 (2006) 3779.
[121] L. Scudiero, D.E. Barlow, K.W. Hipps, J. Phys. Chem. B 104 (2000) 11899.
[122] X. Lu, K.W. Hipps, X.D. Wang, U. Mazur, J. Am. Chem. Soc. 118 (1996) 7197.
[123] K.W. Hipps, X. Lu, X.D. Wang, U. Mazur, J. Phys. Chem. 100 (1996) 11207.
[124] X. Lu, K.W. Hipps, J. Phys. Chem. B 101 (1997) 5391.
[125] K.W. Hipps, D.E. Barlow, U. Mazur, J. Phys. Chem. B 104 (2000) 2444.
[126] D.E. Barlow, K.W. Hipps, J. Phys. Chem. B 104 (2000) 5993.
[127] L. Scudiero, D.E. Barlow, U. Mazur, K.W. Hipps, J. Am. Chem. Soc. 123 (2001) 4073.
[128] L. Scudiero, D.E. Barlow, K.W. Hipps, J. Phys. Chem. B 106 (2002) 996.
[129] P. Sautet, Chem. Rev. 97 (1997) 1097.
[130] T. Lukasczyk, K. Flechtner, L.R. Merte, N. Jux, F. Maier, J.M. Gottfried, H.-P. Steinrueck, J. Phys. Chem. C 111 (2007) 3090.
[131] Z.-C. Dong, A. Kar, P. Dorozhkina, K. Amemiyaa, T. Uchihashia, S. Yokoyama, T. Kamikadob, S. Mashikob, T. Okamoto, Thin Solid Films 438–439 (2003) 262.
[132] D. Fujita, T. Ohgi, W.-L. Deng, H. Nejo, T. Okamoto, S. Yokoyama, K. Kamikado, S. Mashiko, Surface Sci. 454–456 (2000) 1021.
[133] W. Deng, D. Fujita, T. Ohgi, S. Yokoyama, K. Kamikado, S. Mashiko, J. Chem. Phys. 117 (2002) 4995.
[134] Z.-C. Dong, A. Kar, Z.-Q. Zou, T. Ohgi, P. Dorozhkin, D. Fujita, S. Yokoyama, T. Terui, T. Yamada, T. Kamikado, M. Zhou, S. Mashiko, T. Okamoto, Jpn. J. Appl. Phys. 41 (2002) 4898.
[135] Z.-C. Dong, A.S. Trifonov, X.-L. Guo, K. Amemiya, S. Yokoyama, T. Kamikado, T. Yamada, S. Mashiko, T. Okamato, Surface Sci. 532–535 (2003) 237.
[136] X.H. Qiu, G.V. Nazin, W. Ho, Science 299 (2003) 542.
[137] X.-L. Guo, Z.-C. Dong, A.S. Trifonov, K. Miki, Y. Wakayama, D. Fujita, K. Kimura, S. Yokoyama, S. Mashiko, Phys. Rev. B 70 (2004) 233204.
[138] Z.-C. Dong, X.-L. Guo, A.S. Trifonov, P.S. Dorozhkin, K. Miki, K. Kimura, S. Yokoyama, S. Mashiko, Phys. Rev. Lett. 92 (2004) 086801.
[139] X.L. Guo, Z.C. Dong, A.S. Trifonov, K. Miki, K. Kimura, S. Mashiko, Appl. Phys. A 81 (2005) 367.
[140] X.-L. Guoa, Z.-C. Donga, A.S. Trifonova, K. Mikia, K. Kimuraa, S. Mashiko, Appl. Surface Sci. 241 (2005) 28.
[141] V. Balzani, A. Credi, M. Venturi, Molecular Devices and Machines, Wiley-VCH, 2004.
[142] J. Michl, E.C.H. Sykes, ACS Nano 3 (2009) 1042.
[143] V. Balzani, A. Credi, F.M. Raymo, J.F. Stoddart, Angew. Chem. Int. Ed. 39 (2000) 3348.
[144] C.J. Easton, S.F. Lincoln, L. Barr, H. Onagi, Chem. Eur. J. 10 (2004) 3120.
[145] E.R. Kay, D.A. Leigh, F. Zerbetto, Angew. Chem. Int. Ed. 46 (2007) 72.
[146] N. Wintjes, D. Bonifazi, F.Y. Cheng, A. Kiebele, M. Stöhr, T. Jung, H. Spillmann, F. Diederich, Angew. Chem. Int. Ed. 46 (2007) 4089.
[147] M. Wahl, M. Stöhr, H. Spillmann, T.A. Jung, L.H. Gade, Chem. Commun. (2007) 1349.